

AD621751

FURTHER EXPERIMENTAL STUDY
OF PLASMA SHEATH EFFECTS ON ANTENNAS

BY

JOHN M. HAMM
GEORGE TYRAS

CLEARINGHOUSE FOR FEDERAL SCIENTIFIC AND TECHNICAL INFORMATION		
Hardcopy	Microfiche	
\$2.00	\$0.50	44
ARCHIVE COPY		

THE UNIVERSITY OF ARIZONA
COLLEGE OF ENGINEERING
ENGINEERING EXPERIMENT STATION
TUCSON, ARIZONA

PROCESSING COPY

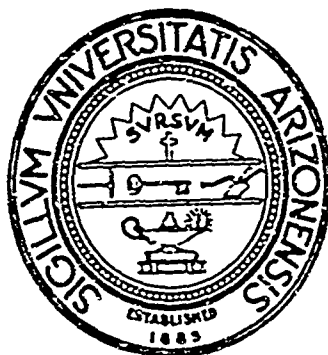
CONTRACT NO. AF 19(628)-3834 ✓
PROJECT 4642
TASK 464202

SCIENTIFIC REPORT NO. 2

JULY 1965

PREPARED FOR

AIR FORCE CAMBRIDGE RESEARCH LABORATORIES
OFFICE OF AEROSPACE RESEARCH
UNITED STATES AIR FORCE
BEDFORD, MASSACHUSETTS



Requests for additional copies by agencies of the Department of Defense, their contractors, and other Government agencies should be directed to:

Defense Documentation Center (DDC)
Cameron Station
Alexandria, Virginia 22314

Department of Defense contractors must be established for DDC services or have their "need-to-know" certified by the cognizant military agency of their project or contract.

All other persons and organizations should apply to the:

Clearinghouse for Federal Scientific
and Technical Information (CFSTI)
Sills Building
5285 Port Royal Road
Springfield, Virginia 22151

FURTHER EXPERIMENTAL STUDY OF PLASMA SHEATH EFFECTS ON ANTENNAS

by

John M. Hamm
and George Tyras

The University of Arizona
College of Engineering
Engineering Experiment Station
Tucson, Arizona

Contract No. AF 19(628)-3834

Scientific Report No. 2

July 1965

Project 4642

Task 464202

PREPARED FOR

Air Force Cambridge Research Laboratories
Office of Aerospace Research
United States Air Force
Bedford, Massachusetts

TABLE OF CONTENTS

Abstract	i
List of Contributors	ii
Related Contracts and Publications	ii
Introduction	1
Theoretical Background	2
Experimental System and Results.	9
Conclusion	13
Figures.	15
References	35

TABLE OF FIGURES

Figures	Page
1 Plasma Clad Slot Antenna Geometry.....	15
2 Models of Plasma Sheath Inhomogeneity Profile: (a) Continuous Model, (b) Four Layers Approximation, (c) Six Layers Approximation.....	16
3 Infinite Inhomogeneous Plasma Sheath Geometry.....	17
4a Experimental Radiation Pattern for Infinite Homogeneous Plasma Sheath.....	18
4b Experimental and Theoretical Radiation -4f Patterns for Semi-Infinite Homogeneous Plasma Sheath.....	19-23
5a Experimental Radiation Pattern for -5b Semi-Infinite Homogeneous Plasma Sheath.....	24-25
6a Experimental Radiation Pattern for -6b Finite Homogeneous Plasma Sheath.....	26-27
7a Admittance Characteristic for Semi- Infinite Homogeneous Plasma Sheath.....	28
7b Admittance Characteristic for Finite Homogeneous Plasma Sheath.....	29
8a Experimental and Theoretical Radiation Patterns for Infinite Inhomogeneous Plasma Sheath (4 Layers).....	30
8b Experimental and Theoretical Radiation Patterns for Infinite Inhomogeneous Plasma Sheath (6 Layers).....	31
9a Semi-Infinite Inhomogeneous -9b Plasma Sheath Geometries.....	32
10 Experimental Radiation Patterns for Semi-Infinite Inhomogeneous Plasma Sheath.....	33
11 Admittance Characteristic for Semi- Infinite Inhomogeneous Plasma Sheath.....	34

ABSTRACT

The plasma sheath simulation technique developed earlier has been used to investigate the effects of various types of sheath discontinuities and inhomogeneities on a slot antenna radiation pattern and input impedance.

In the case of semi-infinite and finite-extent homogeneous plasma sheaths, the radiation pattern and the impedance characteristic are investigated with regard to the geometry of the discontinuity and its proximity to the slot antenna. It is found that the radiation pattern is unaffected by the discontinuity as long as the ratio of the distance between the source and the discontinuity to the sheath thickness is of the order of 20 or greater. When the sheath is made finite in extent, with a discontinuity on each side of the slot, the resulting pattern is seen to be a superposition of the effects of each discontinuity acting separately. The input impedance of the slot exhibits only small variations when the ratio of the discontinuity separation to the sheath thickness is of the order of 4 or greater. For smaller separations, the impedance exhibits significant variations, strongly dependent on the geometry of the discontinuity. The effects produced by inhomogeneities are found to be similar to those of a homogeneous sheath with a certain equivalent dielectric constant.

For both the homogeneous and inhomogeneous sheaths, favorable comparison with the available theory is obtained.

LIST OF CONTRIBUTORS

In addition to the authors, Mr. Lee Cooper and Mr. John Goltz contributed to the research reported in this document. Mr. Cooper and Mr. Goltz are undergraduate Research Assistants in the Department of Electrical Engineering, Engineering Experiment Station, at the University of Arizona in Tucson, Arizona.

RELATED CONTRACTS AND PUBLICATIONS

This document is an extension of the results of Scientific Report No. 1, Contract No. AF 19(628)-3834, December, 1964. This was also published under the title "An Experimental Study of Plasma Sheath Effects on Antennas" in the Journal of Research of the National Bureau of Standards, Radio Science, Vol. 69D, No. 6, June, 1965, pages 839-850.

1. Introduction

The recent interest in propagation of electromagnetic waves through a plasma sheath has generated a large number of papers, mostly theoretical in nature, which solve for the fields of various radiators in the presence of idealized plasma sheath environments. Most of these papers make assumptions concerning the nature of the discontinuities and inhomogeneities in the plasma sheath in order to make the problem more tractable analytically. For example, Tamir and Oliner [1964] approximate a discontinuous plasma sheath by terminating the sheath at a finite distance from the radiator with a termination perpendicular to the ground plane and to the plasma-air interface. As will be seen later, this configuration allows an approximate analytical solution to be made by means of a Kirchhoff-Huygens integration over the discontinuity plane. Rusch [1963] and Tyras [1965b] formulated mathematical models for the dielectric constant in a stratified inhomogeneous medium, with the latter obtaining a closed form expression for the radiation fields.

Little or no experimental work in this area has been reported, primarily due to the handling difficulties and instabilities inherent in actual laboratory plasmas. Recently, however, a plasma sheath environment was successfully simulated using real dielectric materials [Tyras et al., 1965a]. The simulation method allowed the experimental determination of the radiation patterns and input admittances for the problem of a slot antenna in an infinitely conducting plane clad with a homogeneous, lossless, and isotropic plasma layer of infinite extent.

This simulation method provides a laboratory geometry readily suitable for modification so that discontinuities and inhomogeneities in

the plasma sheath may also be simulated. In particular, discontinuities of the "plate" type [Tamir and Oliner, 1964] as well as inhomogeneities composed of discrete vertical stratifications can be easily simulated.

It is the purpose of this report to describe in detail these simulated inhomogeneous and discontinuous plasma sheath environments and to present their respective radiation patterns and input admittances. In the case of the radiation patterns, the experimental results are compared with the approximate analytical results of Tamir and Oliner for the discontinuous plasma sheath and with the asymptotically exact results obtained from a saddle point integration for the inhomogeneous plasma sheath.

2. Theoretical Background

2.1 Semi-Infinite Plasma Sheath

A common idealized model of the plasma sheath surrounding a re-entry vehicle is seen in figure 1, with L_1 and L_2 considered infinite in length. It consists of a perfectly conducting plane covered with a homogeneous plasma of infinite extent. Tamir and Oliner [1962], among others, have analyzed this problem and have shown that the field in the plasma region and the near field in the air region are dominated by a single leaky wave and that the radiation field has a maximum at an angle closely corresponding to the critical angle of geometric optics, as long as the plasma dielectric constant remains positive.

To study the effect of finiteness on the radiation patterns, Tamir and Oliner [1964] proposed the model of figure 1, with L_2 considered infinite, L_1 finite, and $\phi_1 = 90^\circ$. In solving for the approximate radiation fields, it was assumed that the fields incident on the discontinuity plane were just those present in the case of the infinite plasma

slab, namely, the field due to the leaky wave. The problem is then one of an aperture with a prescribed field distribution. A Kirchoff-Huygens integration over the fields on this aperture yields the far field and consequently, the radiation pattern, $R(\theta)$.

$$R(\theta) = |K(\theta)|^2 \quad (1)$$

where

$$K(\theta) = \frac{e^{i(k_p - \sigma)l-1}}{k_p - \sigma} + \frac{e^{i(k_p + \sigma)l-1}}{k_p + \sigma} \cdot e^{i2\sigma} + \frac{ie^{i\sigma}}{\cos(k_{ep})} \left[\frac{\sin(k_{ep} - \sigma)}{k_{ep} - \sigma} + \frac{\sin(k_{ep} + \sigma)}{k_{ep} + \sigma} \right] \quad (2)$$

and where

$$\sigma = kd \cos \theta \quad (k = \text{free space wavenumber})$$

$$l = (L/d) \cot \theta_c \quad (\theta_c = \text{critical angle})$$

$$k_p = k_z d \quad (k_z = \text{transverse wavenumber in the air region})$$

$$k_{ep} = k_{ze} d \quad (k_{ze} = \text{transverse wavenumber in the plasma region})$$

and k_p and k_{ep} satisfy the transverse resonance relation

$$k_p^2 - k_{ep}^2 = (kd)^2 (1 - \epsilon_p) \quad (3)$$

$$\epsilon_p k_p = i k_{ep} \tan k_{ep}$$

When the discontinuity plane and the source are separated by a large distance, the first term in $K(\theta)$ becomes dominant; and the radiation pattern is just that of an infinite plasma layer. Once the ratio of the discontinuity separation to the sheath thickness is made less than 20, the radiation pattern begins to change appreciably. This change is composed of a broadening of the major lobe and a shifting of the peak, all on the discontinuity side of the source ($\theta > 0$). In addition, increased end-fire and broad-side radiation is observed. The exact nature of this change is strongly

dependent upon the plasma sheath parameters (ϵ_p and d).

2.2 Inhomogeneous Plasma Sheath

A possible model for the inhomogeneity profile thought to exist in the plasma sheath surrounding a reentry vehicle is shown in figure 2a. This profile can be approximated, for analytical as well as experimental purposes, by constructing a sheath of discrete layers of homogeneous dielectrics as in figures 2b and 2c. As the layers become finer, the discrete model will approach the continuous model.

Consider, then, an infinitely conducting ground plane covered with N layers of homogeneous dielectric material of infinite extent and excited by an infinite narrow slot antenna, as in figure 3. By symmetry, there is no variation of the fields with the x -coordinate, or $\frac{\partial}{\partial x} = 0$. Consequently, the only component of the magnetic field is the x -component. Then in the n^{th} layer, H_x satisfies the source-free wave equation

$$\nabla^2 H_{x_n} + k_n^2 H_{x_n} = 0 \quad (4)$$

where $k_n = k_0 \sqrt{\epsilon_n}$ and $\nabla^2 = \frac{\partial^2}{\partial z^2} + \frac{\partial^2}{\partial y^2}$. An $e^{-i\omega t}$ time dependence has

been assumed and suppressed throughout. Since the geometry is infinite in the y -direction, a Fourier transform pair on the y -coordinate can be defined as follows:

$$\bar{H}_x = \frac{1}{\sqrt{2\pi}} \int_{-\infty}^{\infty} H_x e^{-i\alpha y} dy \quad (5)$$

$$H_x = \frac{1}{\sqrt{2\pi}} \int_{-\infty}^{\infty} \bar{H}_x e^{i\alpha y} d\alpha. \quad (6)$$

Thus, $\frac{\partial}{\partial y} = i\alpha$ and $\frac{\partial^2}{\partial y^2} = -\alpha^2$, and equation (4) becomes

$$\left[\frac{\partial^2}{\partial z^2} + s_n^2 \right] \bar{H}_{x_n} = 0, \quad (7)$$

where $s_n^2 = k_n^2 - \alpha^2$ and $\text{Im}(s_n) > 0$. The solution of (7) is found to be

$$\bar{H}_{x_n} = A_n e^{is_n z} + B_n e^{-is_n z}; \quad (8)$$

and, by (6)

$$H_{x_n} = \frac{1}{\sqrt{2\pi}} \int_{-\infty}^{\infty} \left[A_n e^{is_n z} + B_n e^{-is_n z} \right] e^{i\alpha y} d\alpha. \quad (9)$$

The A_n and B_n represent the amplitudes of transmitted and reflected waves, respectively. In the air region, there is no reflected wave; and equation (9) becomes

$$H_{x_n} = \frac{1}{\sqrt{2\pi}} \int_{-\infty}^{\infty} A_n e^{is_n(z-d)} e^{i\alpha y} d\alpha. \quad (10)$$

The components of the electric field are given by

$$E_{y_n} = \frac{i}{\omega \epsilon_0 \epsilon_n} \frac{\partial H_{x_n}}{\partial z} \quad (11a)$$

$$E_{z_n} = \frac{-i}{\omega \epsilon_0 \epsilon_n} \frac{\partial H_{x_n}}{\partial y}. \quad (11b)$$

The boundary conditions are the continuity of the tangential E and H fields at the dielectric interfaces and the prescribed E field at the source. This can be summarized by

$$E_{y_{n-1}} = E_{y_n} \quad \text{at } z = d_{n-1} \quad (12a)$$

$$H_{x_{n-1}} = H_{x_n} \text{ at } z = d_{n-1} \quad (12b)$$

and

$$\left. \frac{\partial \psi}{\partial y} \right|_{z=0} = -V_0(y) . \quad (13)$$

Application of (13) on equation (11a) yields

$$V_0(y) = \frac{1}{\omega_{\epsilon_0 \epsilon_1}} \cdot \frac{1}{\sqrt{2\pi}} \int_{-\infty}^{\infty} s_1(A_1 - B_1) e^{i\alpha y} d\alpha . \quad (14)$$

Thus the quantity $s_1(A_1 - B_1)$ is recognized as the Fourier transform of $\omega_{\epsilon_0 \epsilon_1} V_0(y)$; or, from equations (5) and (6) ,

$$s_1(A_1 - B_1) = \frac{1}{\sqrt{2\pi}} \int_{-\infty}^{\infty} \omega_{\epsilon_0 \epsilon_1} V_0(y) e^{-i\alpha y} d\alpha .$$

Thus

$$A_1 - B_1 = \frac{\omega_{\epsilon_0 \epsilon_1} V}{\sqrt{2\pi}} \cdot \frac{1}{s_1} , \quad (15a)$$

which can be rewritten as

$$A_1 = \frac{\omega_{\epsilon_0 \epsilon_1} V}{\sqrt{2\pi}} \cdot \frac{1}{s_1} \left[\frac{1}{1 - (B_1/A_1)} \right] \quad (15b)$$

Using the boundary conditions for the intermediate interfaces, equations (12a) and (12b) become

$$A_n e^{i s_n d_{n-1}} + B_n e^{-i s_n d_{n-1}} = A_{n-1} e^{i s_{n-1} d_{n-1}} + B_{n-1} e^{-i s_{n-1} d_{n-1}} \quad (16a)$$

$$\frac{s_n}{\epsilon_n} \left[A_n e^{i s_n d_{n-1}} - B_n e^{-i s_n d_{n-1}} \right] = \frac{s_{n-1}}{\epsilon_{n-1}} \left[A_{n-1} e^{i s_{n-1} d_{n-1}} - B_{n-1} e^{-i s_{n-1} d_{n-1}} \right] . \quad (16b)$$

The application of equations (16) at the last interface, where $B_N = 0$, results in the following expressions:

$$\frac{A_{N-1}}{B_{N-1}} = \frac{-l_N}{m_N} e^{-12s_{N-1}d} \quad (17a)$$

and

$$A_N = \frac{2s_{N-1}\epsilon_N}{l_N} e^{is_{N-1}d} A_{N-1} \quad (17b)$$

where

$$l_n = s_n \epsilon_{n-1} + s_{n-1} \epsilon_n \quad \text{and}$$

$$m_n = s_n \epsilon_{n-1} - s_{n-1} \epsilon_n$$

Equations (16) can now be manipulated into the following recursion relationships:

$$\frac{A_{n-1}}{B_{n-1}} = e^{-2is_{n-1}d} \left[\frac{\frac{A_n}{B_n} e^{-is_{n-1}d} - \frac{l_n}{m_n} e^{is_{n-1}d}}{\frac{A_n}{B_n} e^{is_{n-1}d} - \frac{l_n}{m_n} e^{-is_{n-1}d}} \right] \quad (18)$$

and

$$A_n = \frac{2s_{n-1}\epsilon_n A_{n-1} e^{is_{n-1}d}}{l_n e^{is_{n-1}d} - \frac{B_n}{A_n} m_n e^{-s_{n-1}d}} \quad (19)$$

These recursion relationships can now be programmed on a computer to yield the desired transmission coefficient, A_N . The procedure for calculating A_N was the following:

1. $\frac{A_{N-1}}{B_{N-1}}$ and its reciprocal were calculated from equation (17a) and were stored.
2. The result was put into equation (18), where a series of iterations were performed to calculate $\frac{A_{N-2}}{B_{N-2}}, \dots, \frac{A_1}{B_1}$. Each $\frac{A_n}{B_n}$ and its reciprocal were stored.
3. A_1 was then calculated using equation (15b). This result was then placed in equation (19), where iterations were performed to obtain A_2, \dots, A_{N-1} .
4. A_N was then obtained from equation (17b).

Evaluation of the integral representation of the transmitted field can now be carried out by making the following changes of the variables in equation (7):

$$\begin{aligned} y &= \rho \sin \theta \\ z-d &= \rho \cos \theta \\ \alpha &= k_0 \sin \phi \end{aligned}$$

If the last medium is air, then $\epsilon_N = 1$ and equation (10) becomes:

$$H_{xN} = \frac{1}{\sqrt{2\pi}} \int A_N e^{ik_0 \rho \cos(\theta-\phi)} k_0 \cos \phi \, d\phi. \quad (20)$$

The method of saddle point integration is used to evaluate this expression for the radiation field. The resulting expression is:

$$H_{xN} = e^{i(k_0 \rho - \pi/4)} \sqrt{\frac{k_0}{\rho}} \cos \theta \, A_N \Big|_{\phi = \theta}. \quad (21)$$

Since A_N is ultimately evaluated at $\phi = \theta$, the value of each s_n used in the computer program is just $s_n = k_0 \sqrt{\epsilon_n - \sin^2 \theta}$.

3. Experimental Systems and Results

3.1 Discontinuous Plasma Sheath

The plasma sheath simulation system described by Tyras et al. [1965a] replaced the problem of the plasma-air interface with that of an air-liquid dielectric interface. The dielectric used was Aroclor 1232, a fluid with a dielectric constant of 2.78 and a low loss tangent. The fluid was contained in a semi-cylindrical plexiglass tank with a dielectric constant of 2.59. This provided an essentially reflection-free plexiglass-aroclor interface. It was shown then that the air layer between the ground plane and the tank was equivalent to a plasma sheath with a dielectric constant of 0.36, and that the Aroclor region was equivalent to the air region above the plasma sheath. Thus the radiation patterns obtained for the experimental system were expected to exhibit the same functional relationships as those obtained from the analytical solution of the actual problem.

That this was a feasible method for a plasma sheath simulation was shown by the excellent agreement between the theoretical and experimental radiation patterns. The variation of the input admittance with the sheath thickness was also investigated, and good agreement with the available theoretical data was again observed.

The extension of this method to simulate finite and semi-infinite plasma sheath environments is straightforward. A plexiglass sheet was placed in the space between the tank and the ground plane in order to simulate the rectangular semi-infinite plasma sheath of figure 1, with L_2 considered infinite and ϕ_1 equal to 90° . Radiation patterns were then obtained for various values of the discontinuity separation L_1 . Similar measurements were also made for angular discontinuities with ϕ_1 equal to

45° and 15° . It is expected that this type of discontinuity is a more realistic model of the environments encountered in reentry.

Figures 4a through 4f show the experimental and theoretical radiation patterns obtained for the rectangular discontinuity. The features of major importance in these patterns are the following:

1. The radiation pattern is relatively unaffected as long as the ratio of the discontinuity separation to the sheath thickness is at least 20.
2. As the discontinuity plane is moved closer to the source, the major lobe of the radiation pattern on the discontinuity side of the source ($\theta > 0$) is seen to broaden and the critical angle is seen to shift. In addition, increased broadside and end-fire radiation is observed.
3. While it is not shown on all the figures, the radiation pattern on the other side of the source ($\theta < 0$) is affected very little by the presence of the discontinuity.

These features are completely in line with the predictions of Tamir and Oliner [1964] on the basis of their leaky-wave analysis.

In comparing the theoretical and experimental radiation patterns, it is to be noted that no outstanding point-by-point agreement was reached. This is due in part to the inherent errors arising from the approximate leaky-wave method of analysis for obtaining the radiation fields. This error is usually apparent at broadside for certain combinations of plasma dielectric constant, ϵ_p , and sheath thickness, d , which is readily apparent in figure 4b. However, the general qualitative nature of the effects of

the discontinuity on the radiation patterns is in good agreement with the theory in view of the three features noted above.

With a view toward simulating more realistic discontinuities, the geometry of figure 1, with finite L_1 and L_2 , was also investigated. It was observed that the effects of the angular discontinuities were of the same general type as those of the rectangular discontinuity. Again, no appreciable changes were noticed for separations greater than 10 wavelengths; and the changes noted for smaller separations were of the same type as those observed previously. Figures 5a and 5b show the radiation patterns obtained for an angular discontinuity with L_2 infinite and $\phi_1 = 45^\circ$. The effect of the addition of a second discontinuity to simulate the environment of figure 1 is seen in figures 6a and 6b. It is evident that the resulting radiation pattern is essentially a superposition of the effects of each discontinuity acting separately.

The effects of discontinuities on the input admittance were also investigated. Measurements were made at the input to the tapered waveguide section of the antenna, exactly as reported earlier [Tyras et al., 1965a]. The resulting admittance characteristics are seen in figures 7a and 7b. Figure 7a shows the variation of input admittance with the discontinuity separation with only one discontinuity present. It is seen that the conductance remains essentially constant if the ratio of the discontinuity separation to the sheath thickness is at least 4, while the susceptance remains constant over the whole range of the variation in L_1 . The effect of the second discontinuity on the input admittance is seen in figure 7b.

3.2 Inhomogeneous Plasma Sheath

As mentioned in Section 2.2, the discrete-layered model for the inhomogeneous plasma sheath is a convenient one analytically as well as experimentally. The profiles shown in figures 2b and 2c are easily simulated in the laboratory using the earlier scaling technique [Tyras et al., 1965a]. Table I below shows the properties of the various materials used to simulate these profiles.

Table I

(Data for 25°C and $3 \times 10^9 - 1 \times 10^9$ cps)

<u>Material</u>	<u>Actual ϵ</u>	<u>Scaled ϵ</u>
Styrofoam	1.00	0.360
Teflon	2.08	0.748
Polyethylene	2.25	0.813
Polystyrene	2.54	0.913
Plexiglass	2.59	0.935

Figures 8a and 8b show the theoretical and experimental radiation patterns obtained for these two profiles. In figure 8a, good agreement with theory is observed, with the main discrepancy occurring in the slightly different critical angles. In figure 8b, a difference of 2 db is noted in the attenuation at broadside, while there is excellent agreement at the critical angle. In each of these figures, the most significant point to observe is the general shape of the radiation patterns. It seems to indicate that an inhomogeneous plasma sheath of the type shown in figures 2b and 2c acts effectively like a homogeneous plasma sheath with some average dielectric constant. This average value of ϵ_p can be readily computed from the relation, $\sin^2 \theta_c = \epsilon_p$, where θ_c is the critical angle obtained from the radiation pattern. This should hold at least as long as the minimum value of the dielectric constant in the sheath remains positive.

The effects of discontinuities in the inhomogeneous plasma sheath were also investigated. The configurations of figures 9a and 9b were simulated in the laboratory using the materials of Table I. The radiation patterns for various values of the discontinuity separation, L_1 , are seen in figure 10. These patterns exhibit the same characteristics as those of the discontinuous homogeneous sheath.

The input admittance of the antenna in the presence of these semi-infinite, inhomogeneous environments was also obtained. Figure 11 shows the conductance and susceptance as a function of the discontinuity separation. As noted before in the case of the homogeneous sheath, the variation is very slight for separation-to-thickness ratios of 4 and larger. It is only when the discontinuity is situated closer to the source that significant variations are observed.

4. Conclusions

The extension of the earlier results [Tyras et al., 1965a] to include more realistic radiating system environments has succeeded in predicting the qualitative effects of the discontinuities and inhomogeneities in the plasma sheath on the radiation patterns and input admittances. In the case of the finite and semi-infinite homogeneous plasma sheath, it has been shown that the analytically approximate method of Tamir and Oliner [1964] is a valid one to use in order to predict the essential features of the radiation pattern. It was observed that the radiation pattern was relatively unaffected if the discontinuity separation-to-sheath thickness ratio was about 20 or greater. For smaller separations, the radiation pattern was observed to broaden and the major lobe to shift. In the case of a stratified inhomogeneous sheath, this report has shown that the

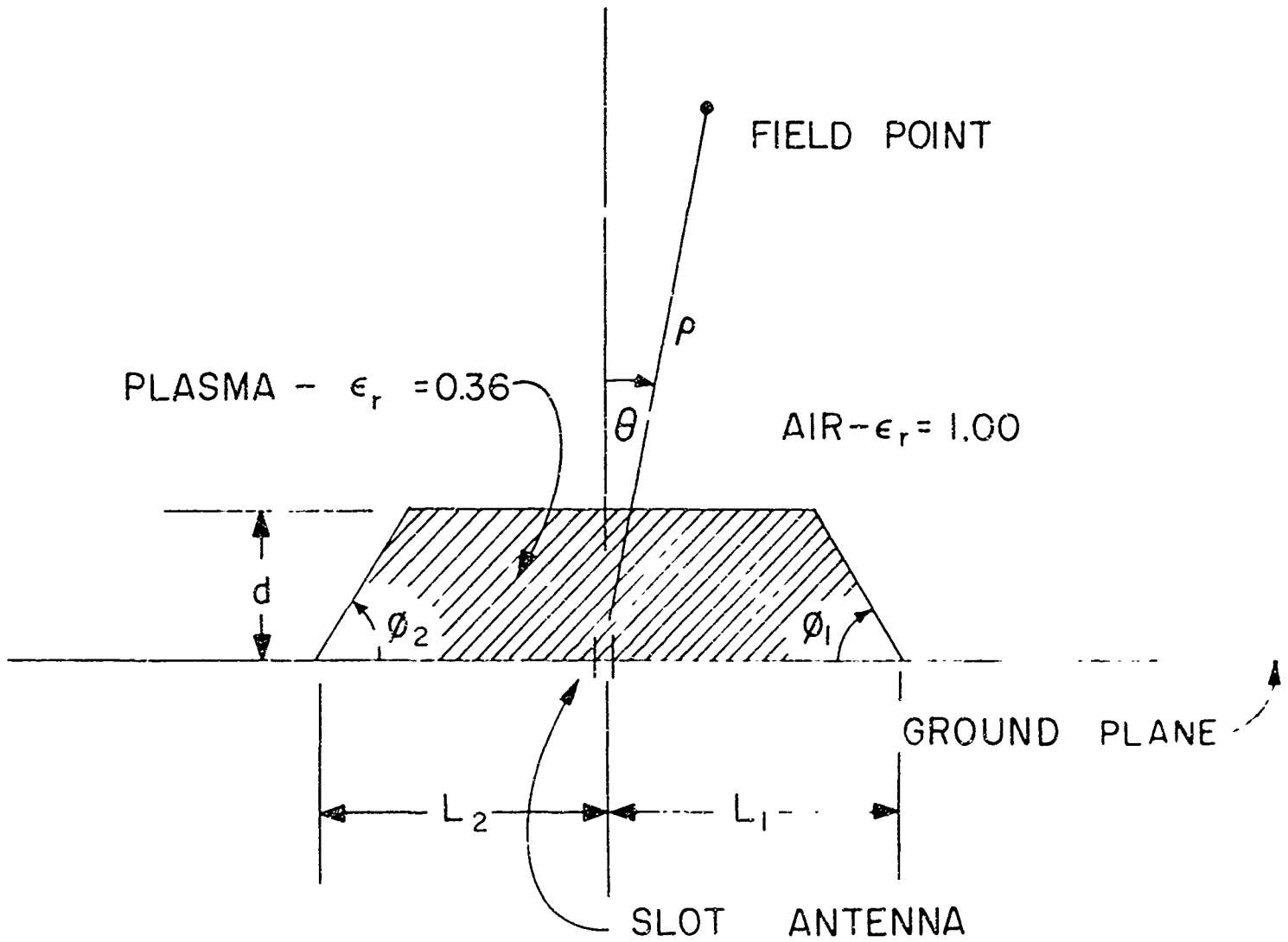


Fig. 1. Plasma Clad Slot Antenna Geometry

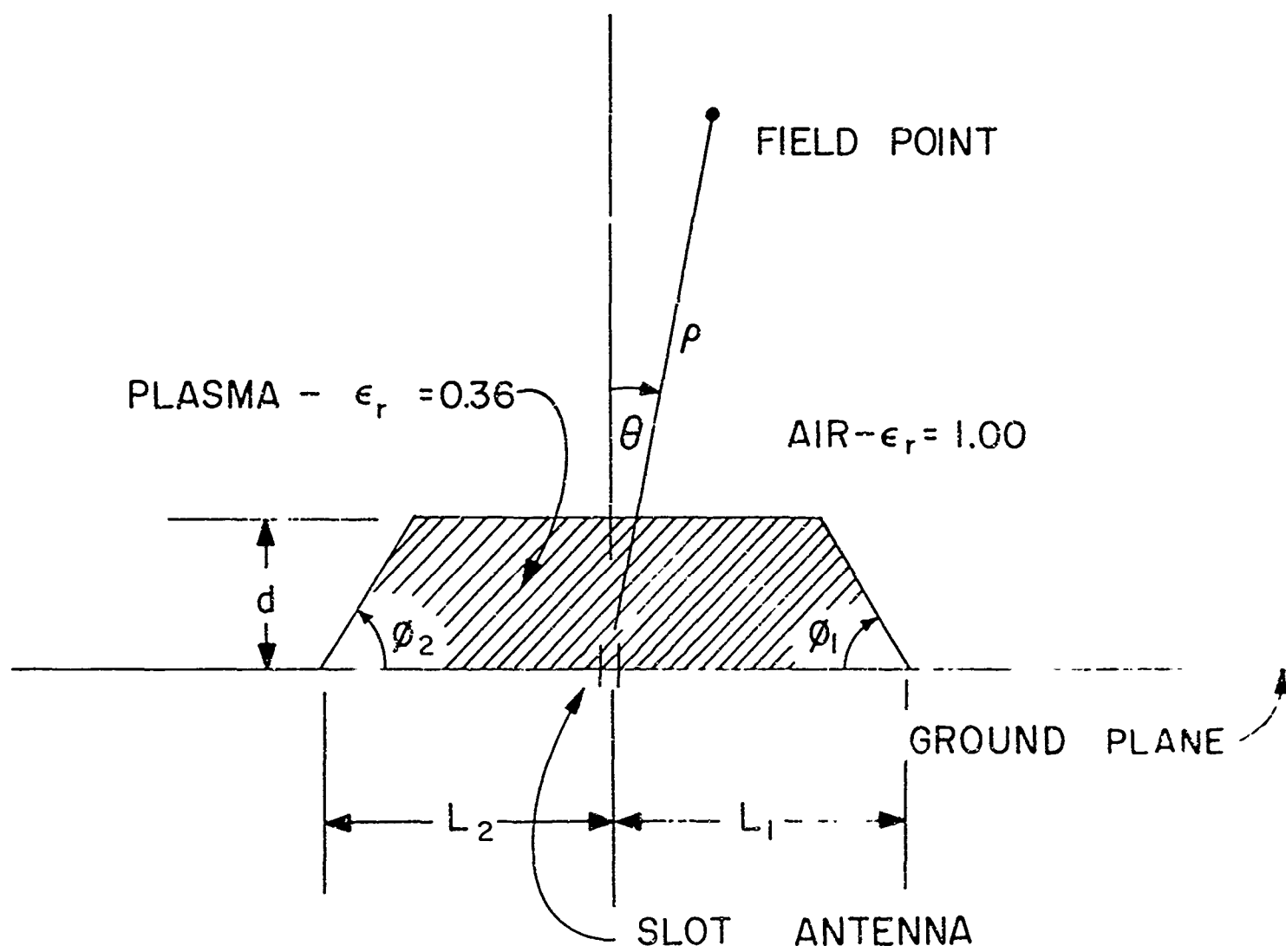


Fig. 1. Plasma Clad Slot Antenna Geometry

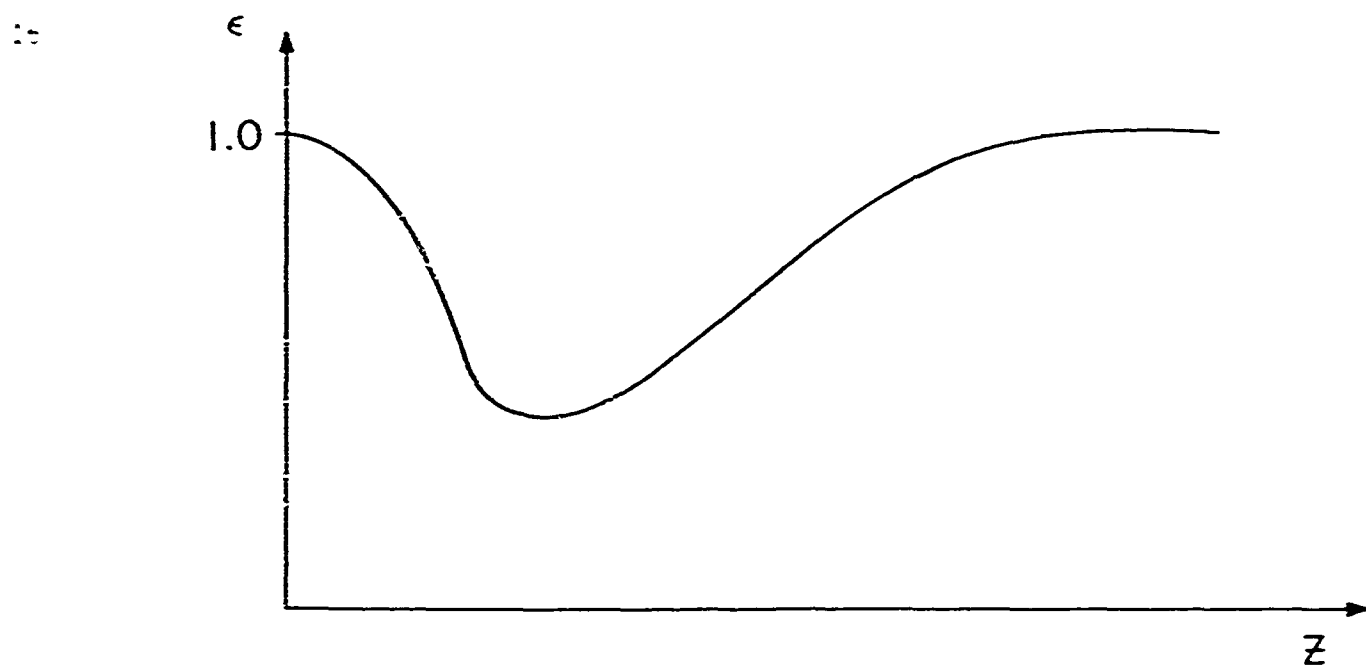


Fig. 2a

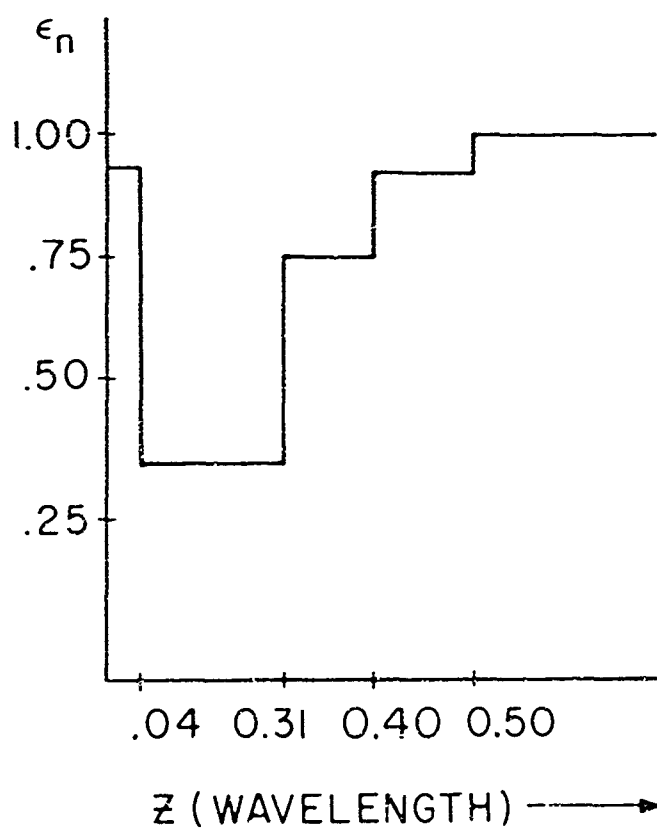


Fig. 2b

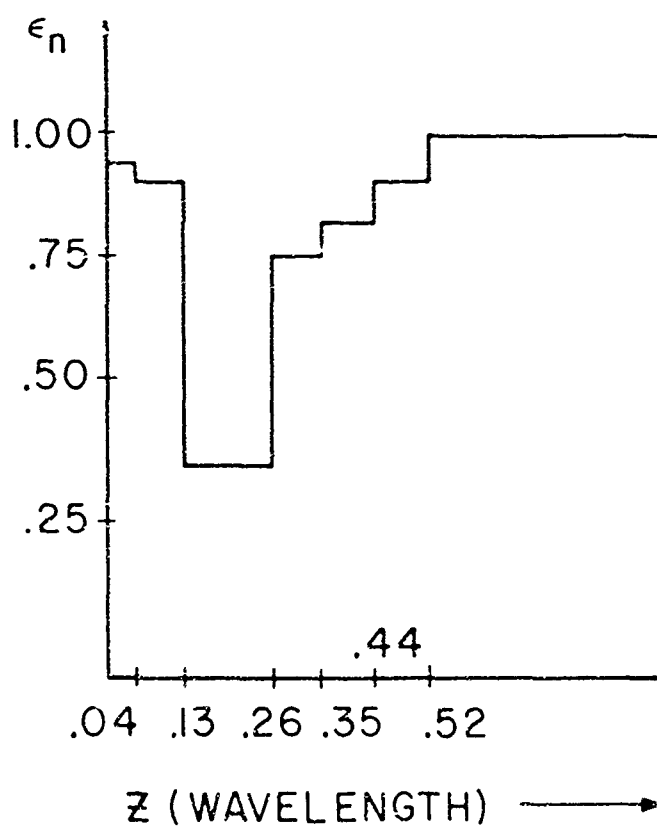


Fig. 2c

Fig. 2 Models of Plasma Sheath Inhomogeneity Profile: (a) Continuous Model, (b) Four Layers Approximation, (c) Six Layers Approximation

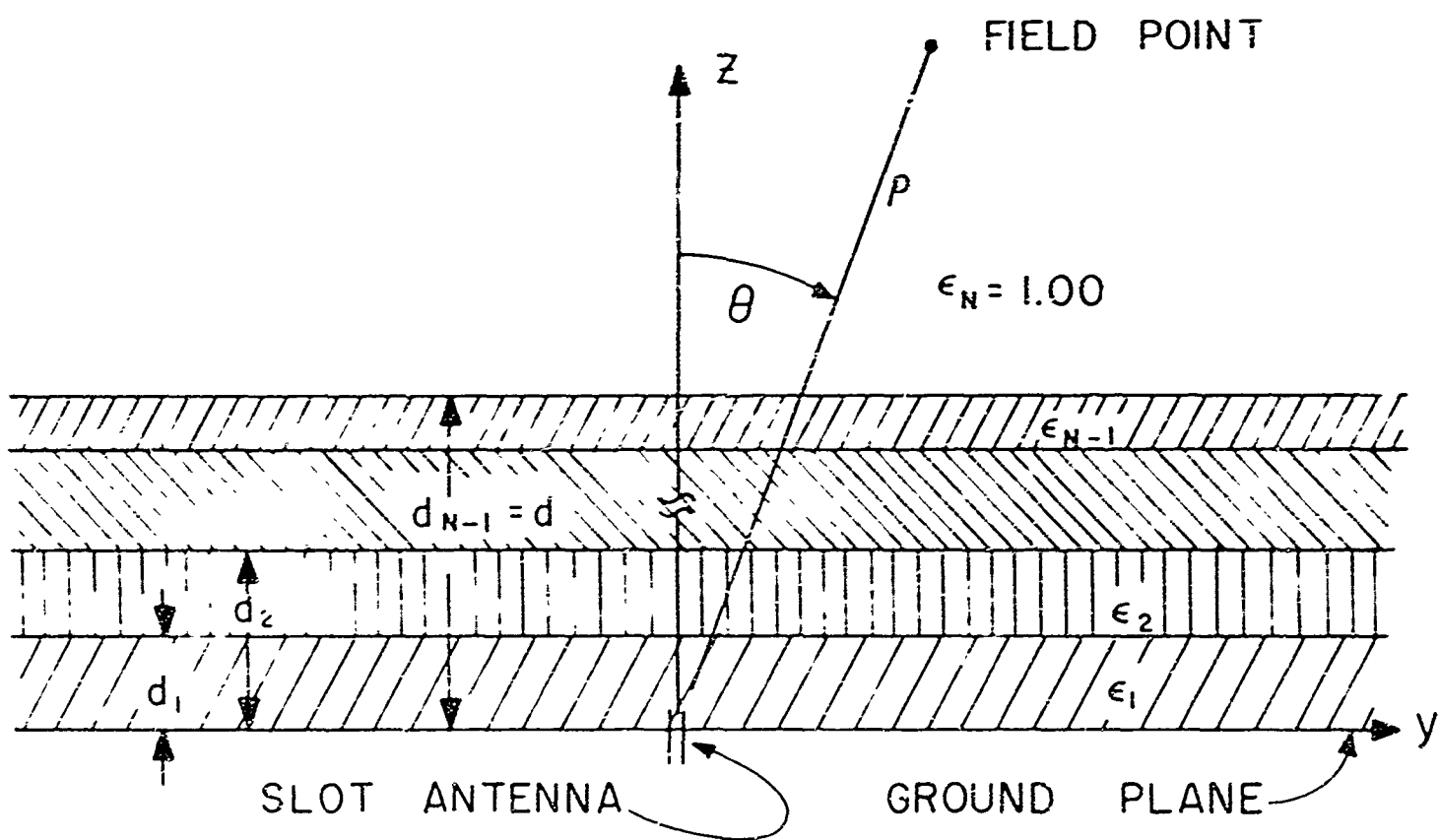


Fig. 3. Infinite Inhomogeneous Plasma Sheath Geometry

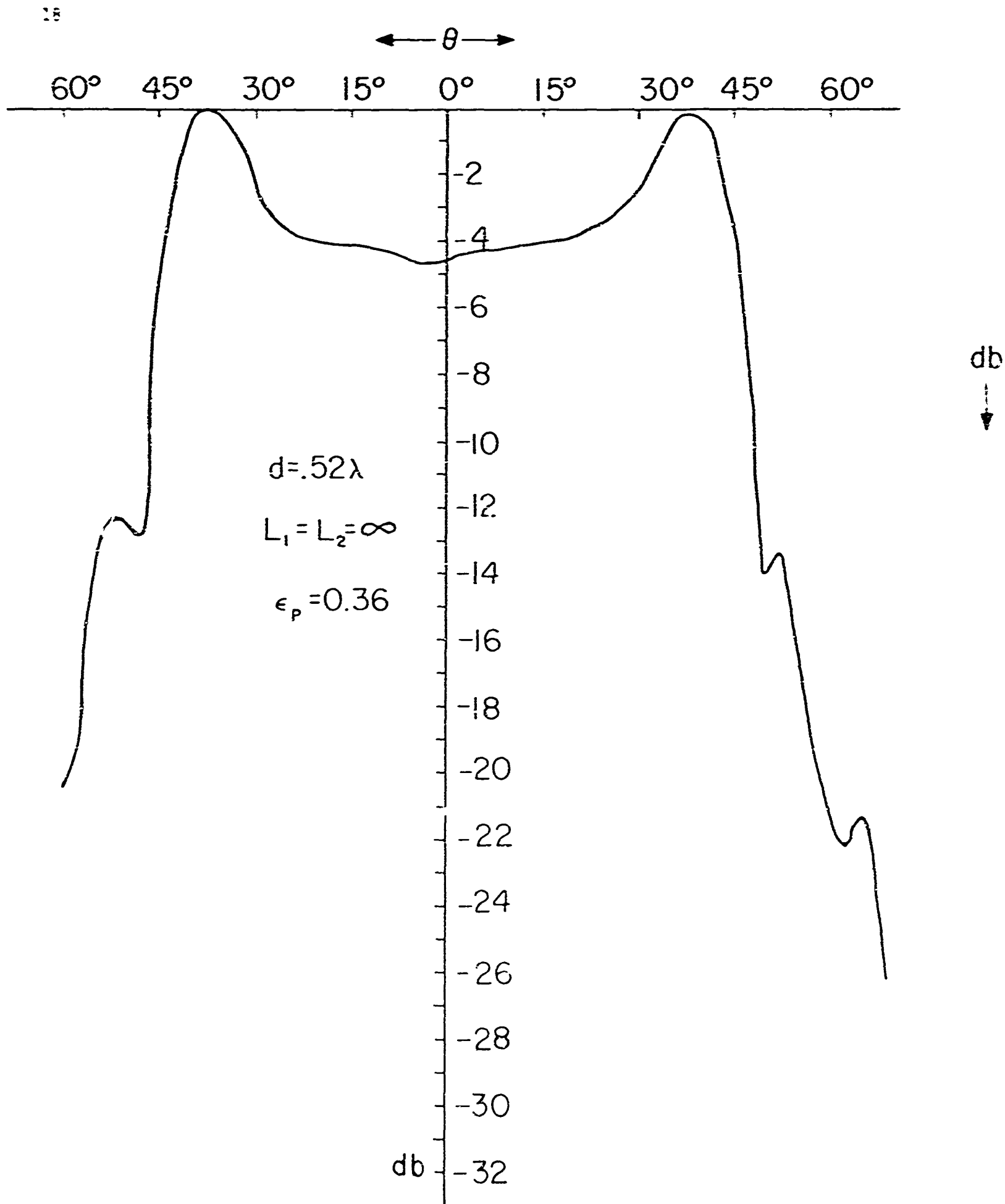


Fig. 4a Experimental Radiation Pattern for Infinite Homogeneous Plasma Sheath

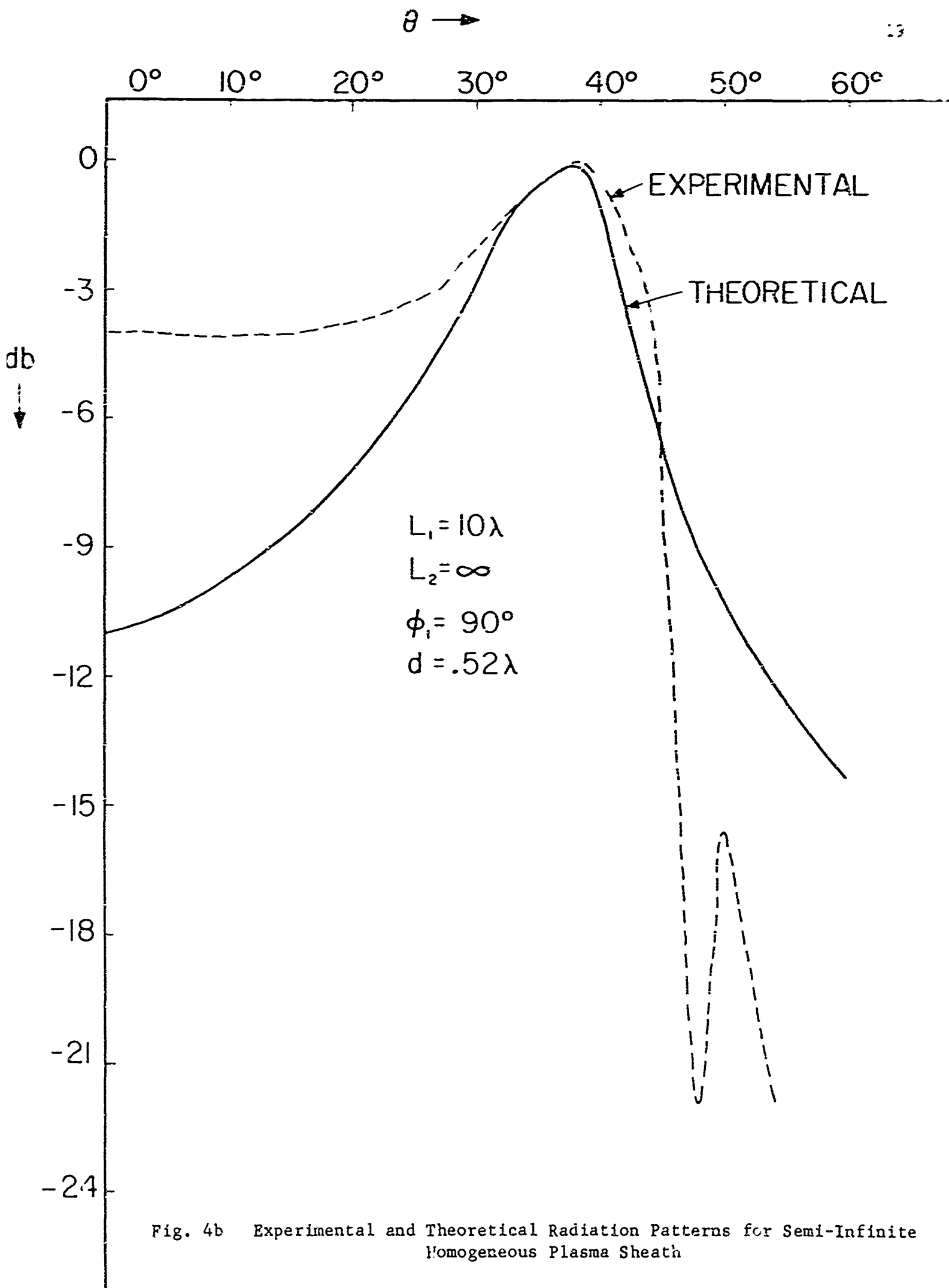


Fig. 4b Experimental and Theoretical Radiation Patterns for Semi-Infinite Homogeneous Plasma Sheath

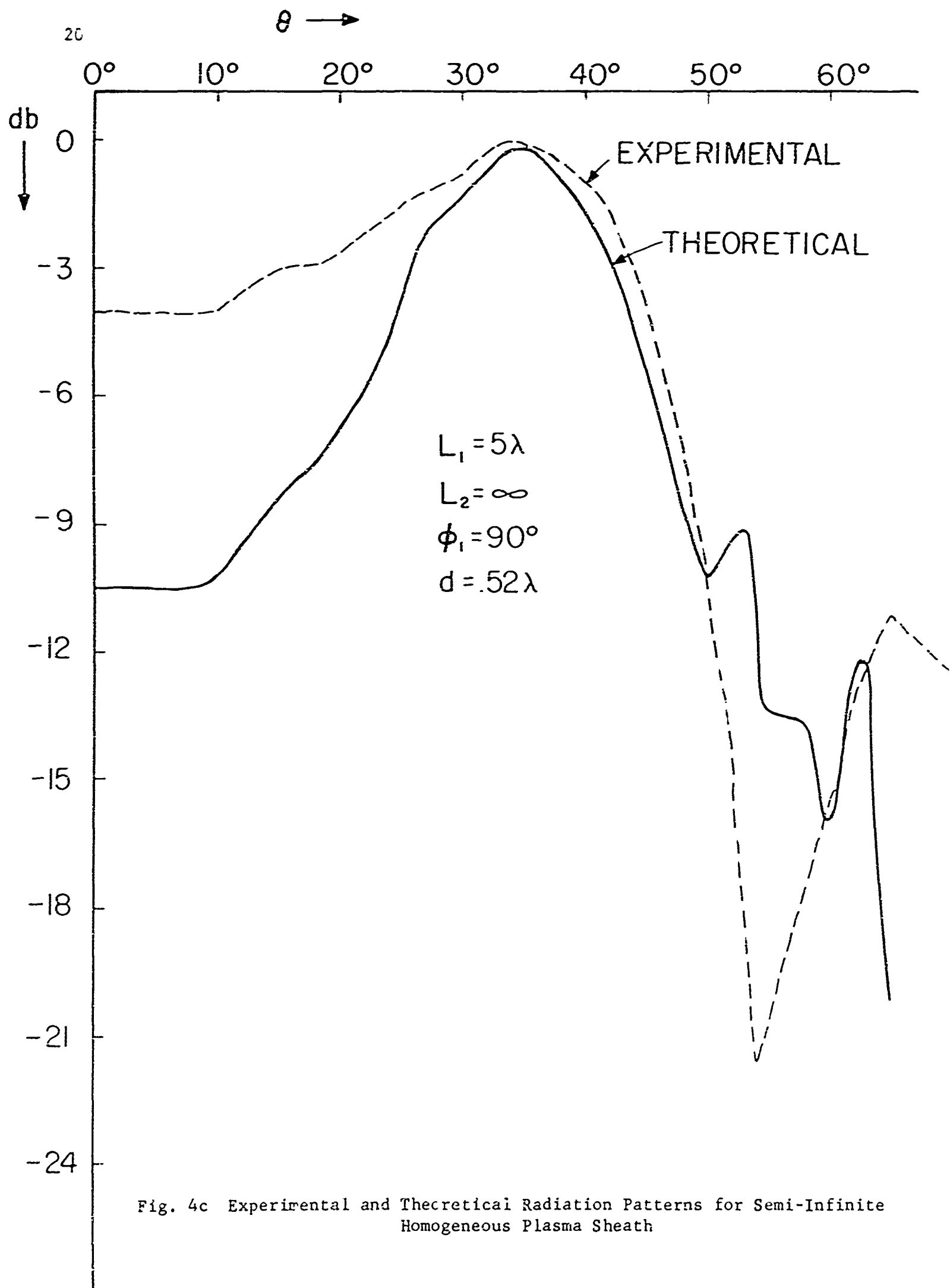


Fig. 4c Experimental and Theoretical Radiation Patterns for Semi-Infinite Homogeneous Plasma Sheath

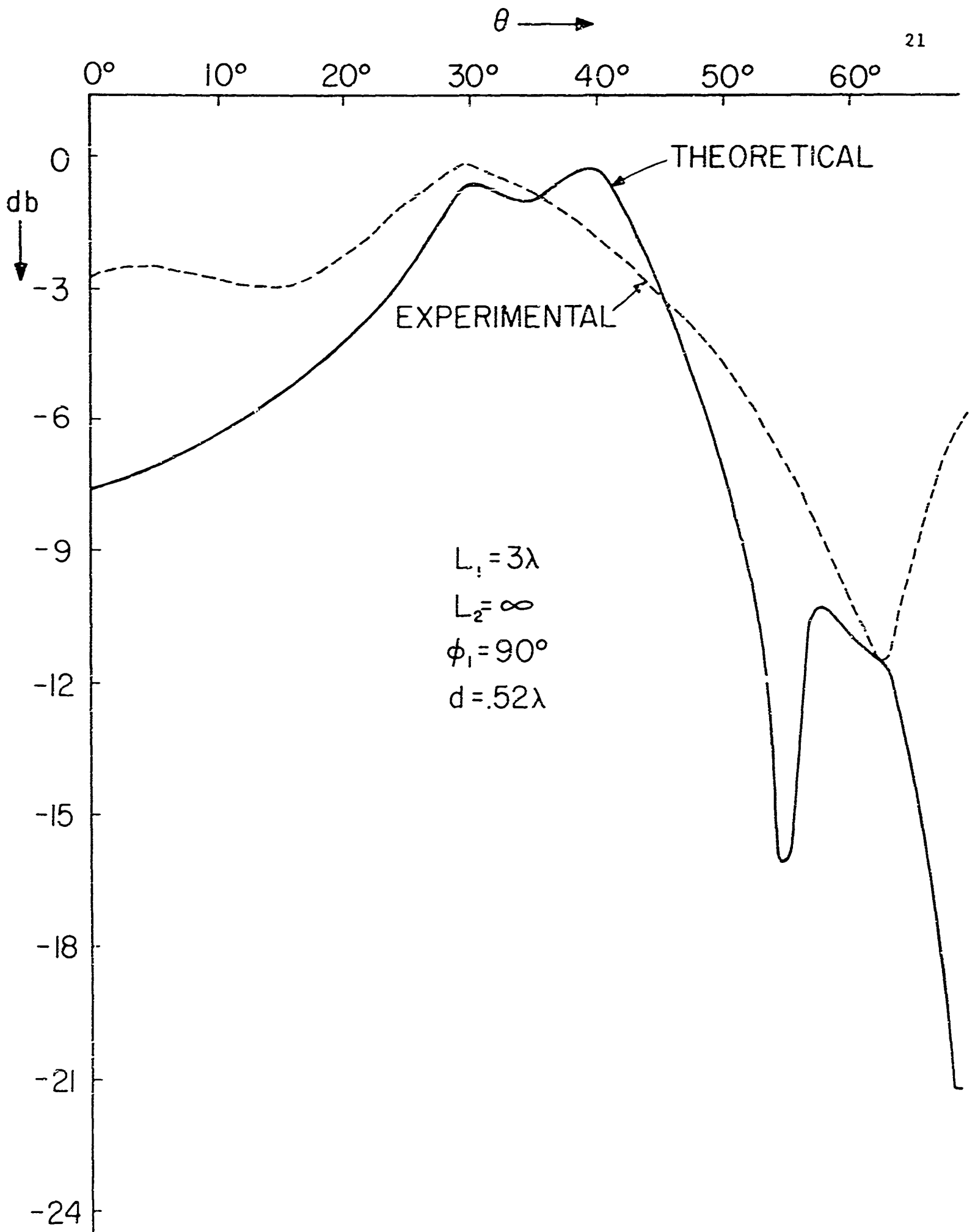


Fig. 4d Experimental and Theoretical Radiation Patterns for Semi-Infinite Homogeneous Plasma Sheath

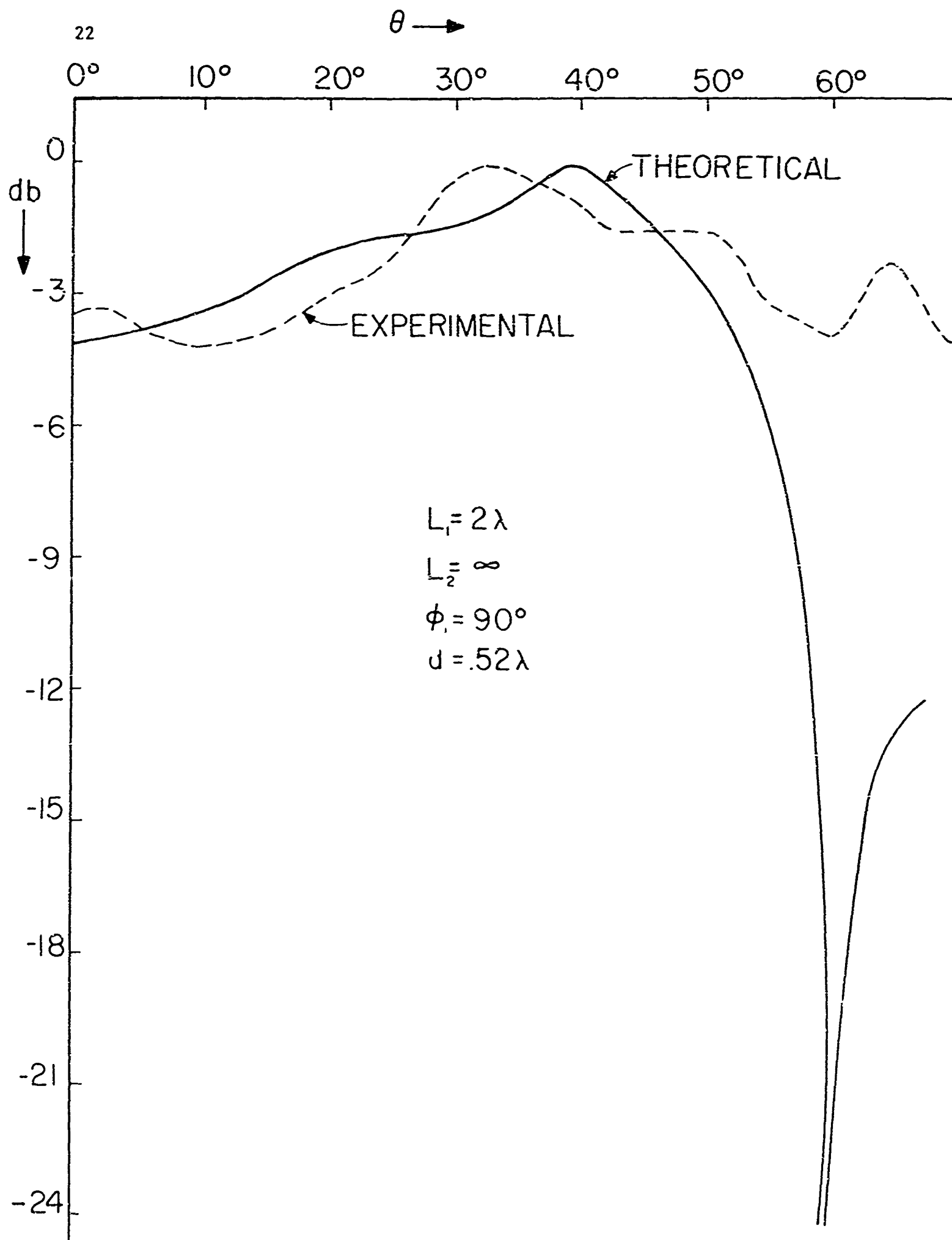


Fig. 4e Experimental and Theoretical Radiation Patterns for Semi-Infinite Homogeneous Plasma Sheath

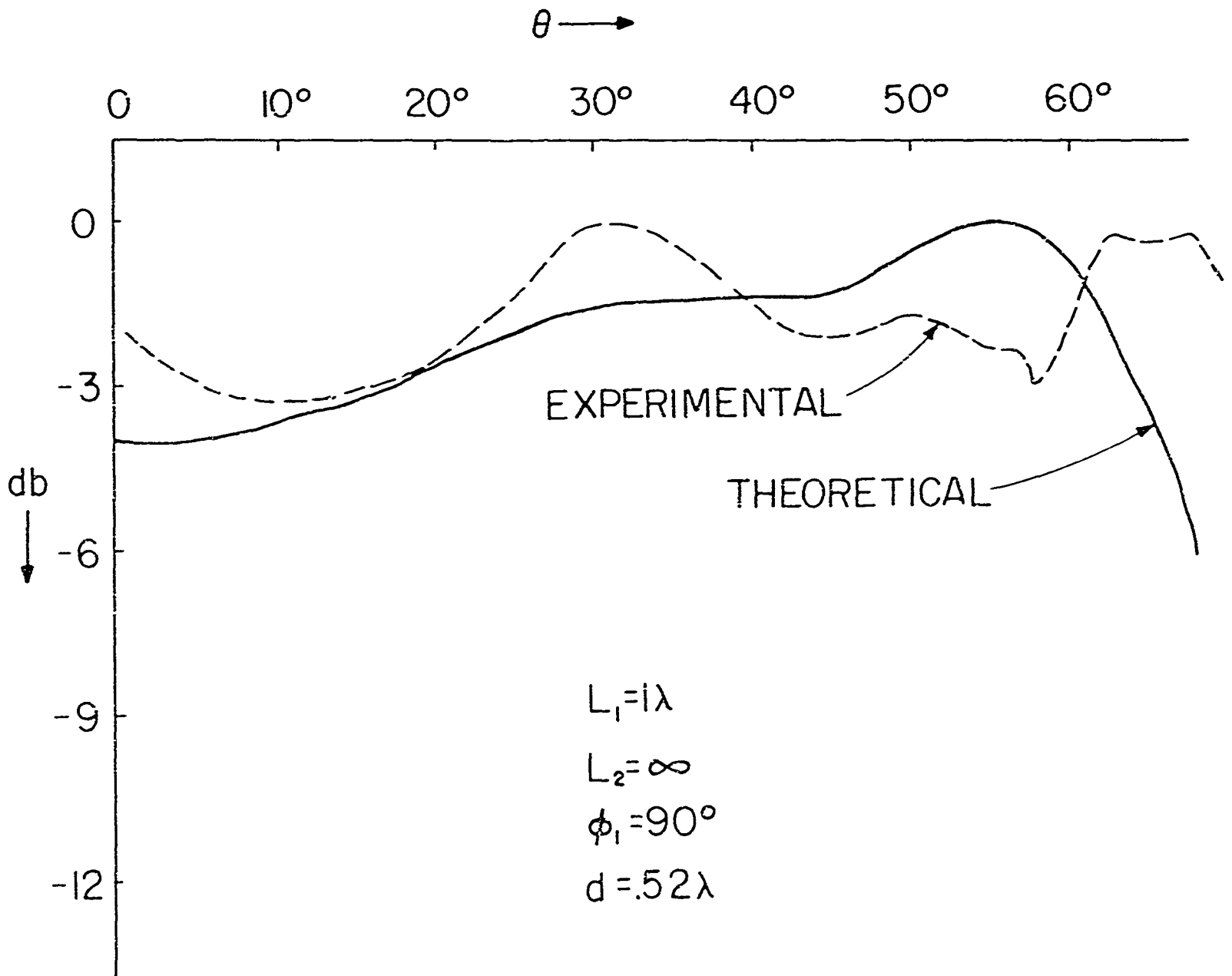


Fig. 4f Experimental and Theoretical Radiation Patterns for Semi-Infinite Homogeneous Plasma Sheath

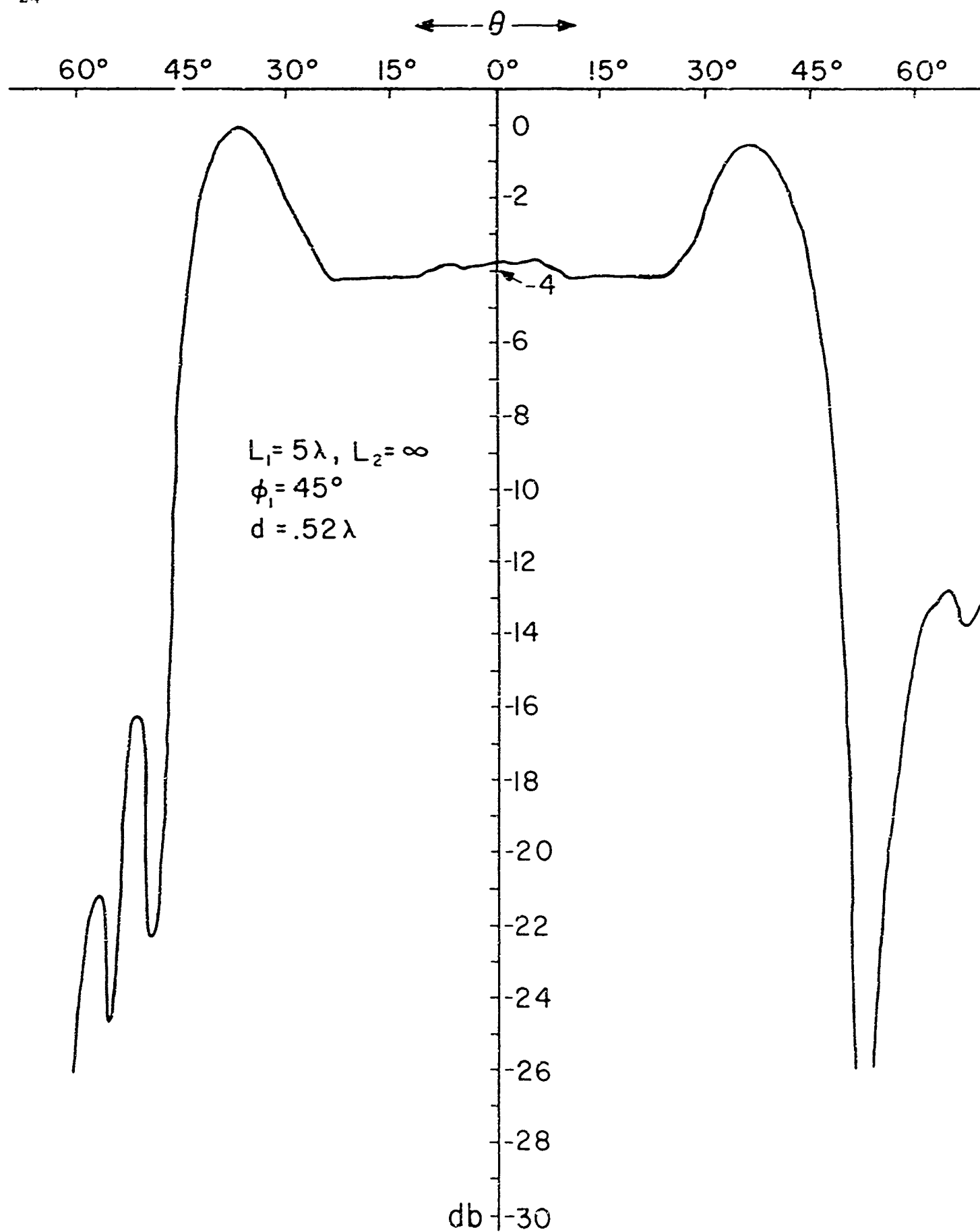


Fig. 5a Experimental Radiation Pattern for Semi-Infinite Homogeneous Plasma Sheath

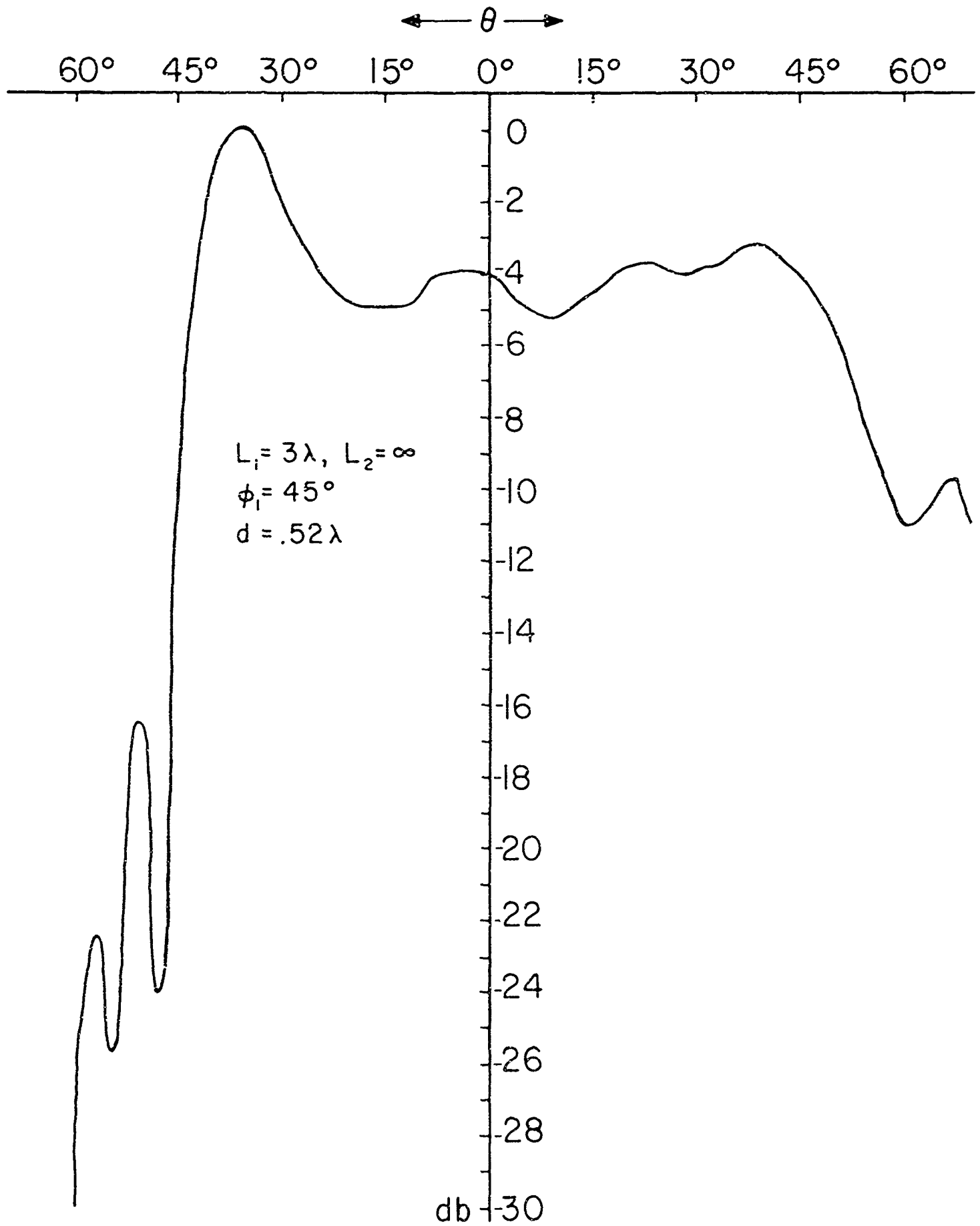


Fig. 5b Experimental Radiation Pattern for Semi-Infinite Homogeneous Plasma Sheath

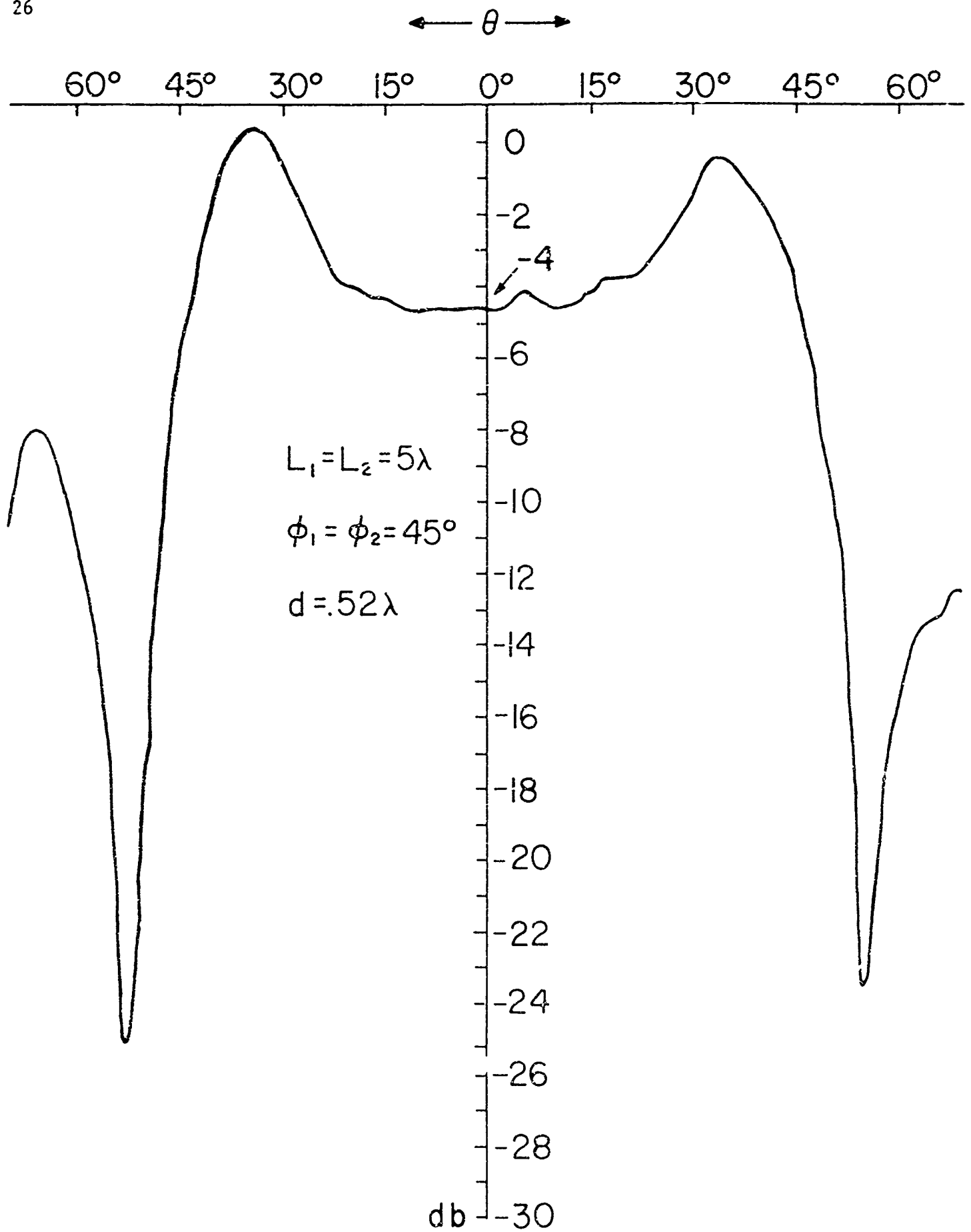


Fig. 6a Experimental Radiation Pattern for Finite Homogeneous Plasma Sheath

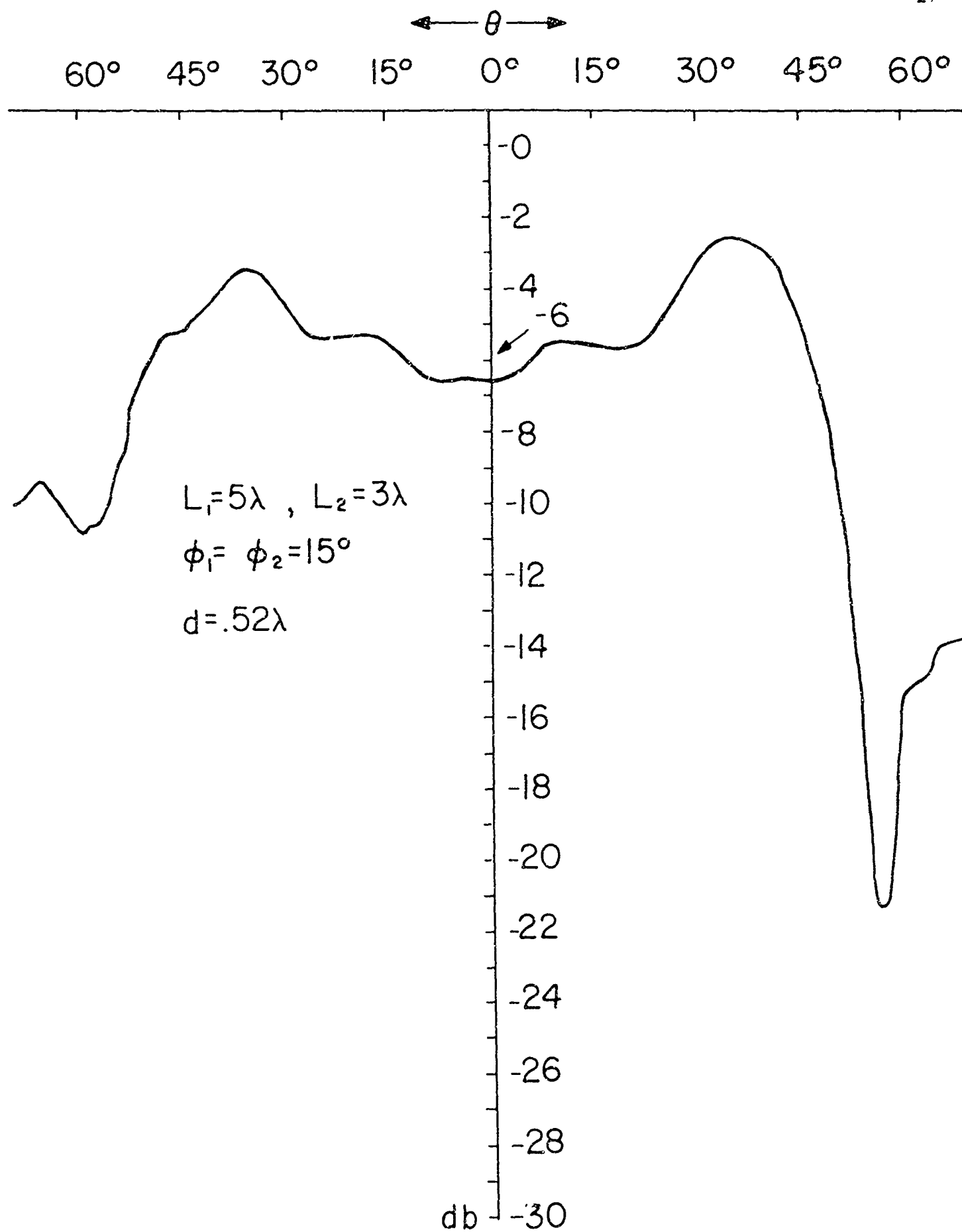


Fig. 6b Experimental Radiation Pattern for Finite Homogeneous Plasma Sheath

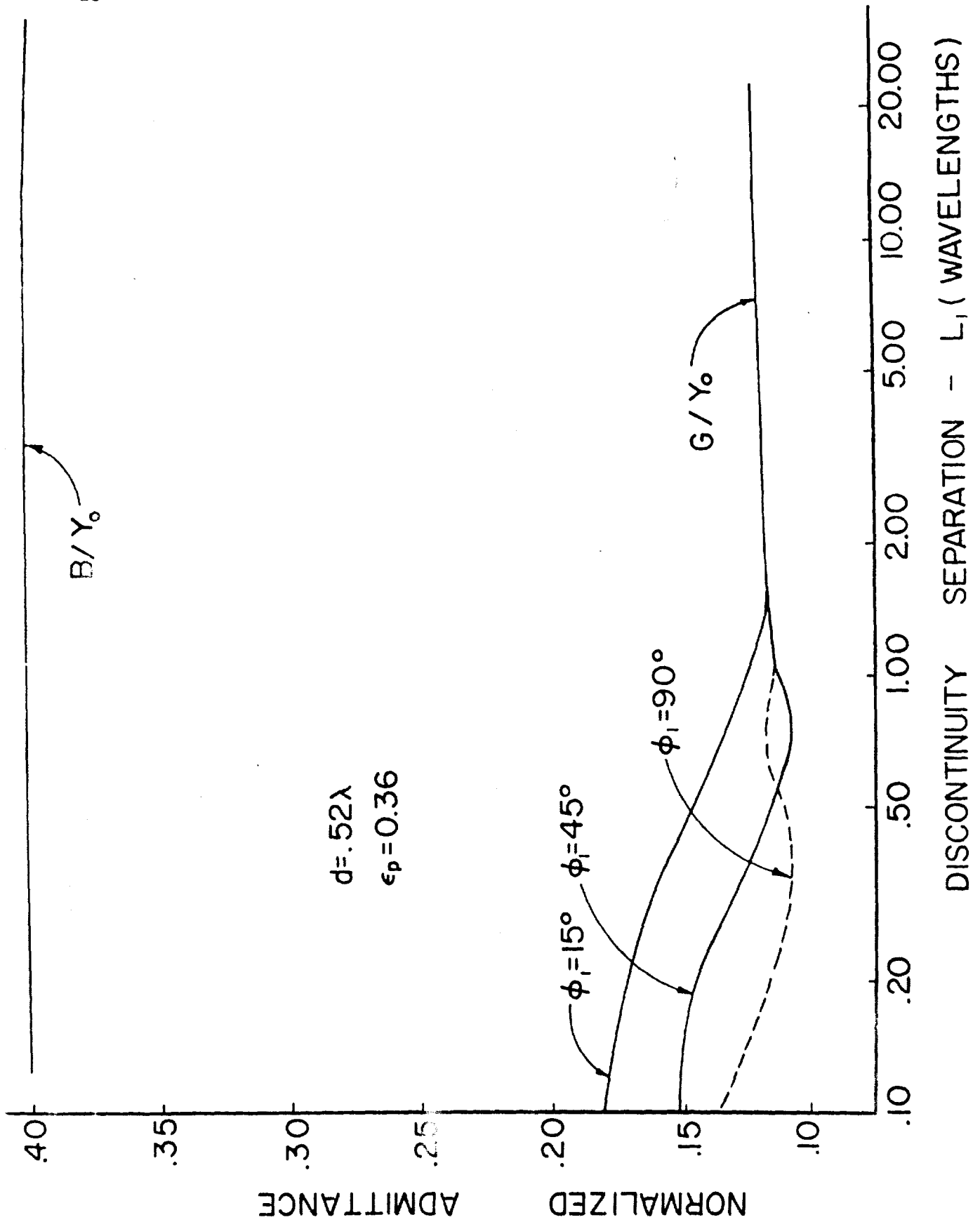


Fig. 7a Admittance Characteristic for Semi-Infinite Homogeneous Plasma Sheath

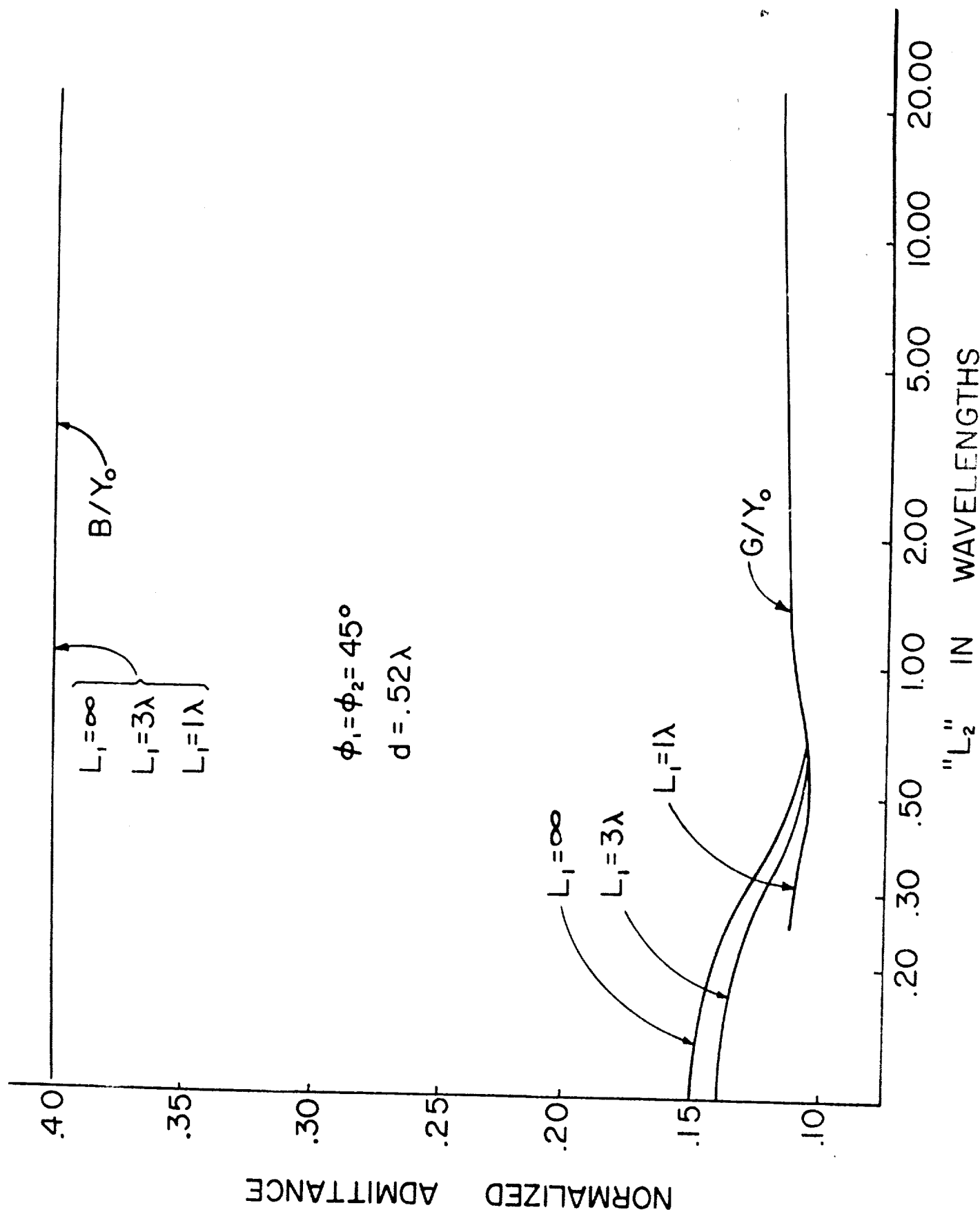


Fig. 7b Admittance Characteristic for Finite Homogeneous Plasma Sheath

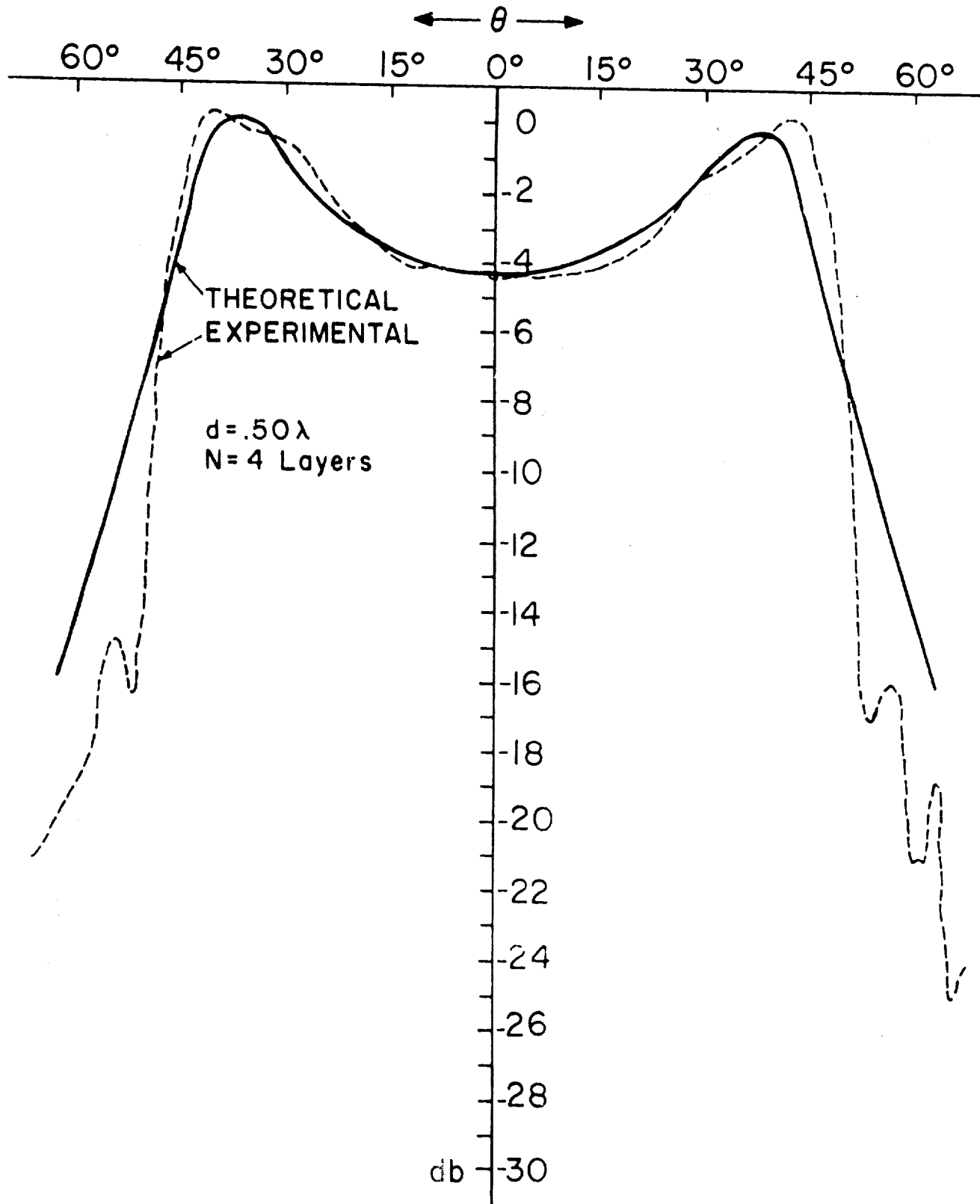


Fig. 8a Experimental and Theoretical Radiation Patterns for Infinite Inhomogeneous Plasma Sheath (4 Layers)

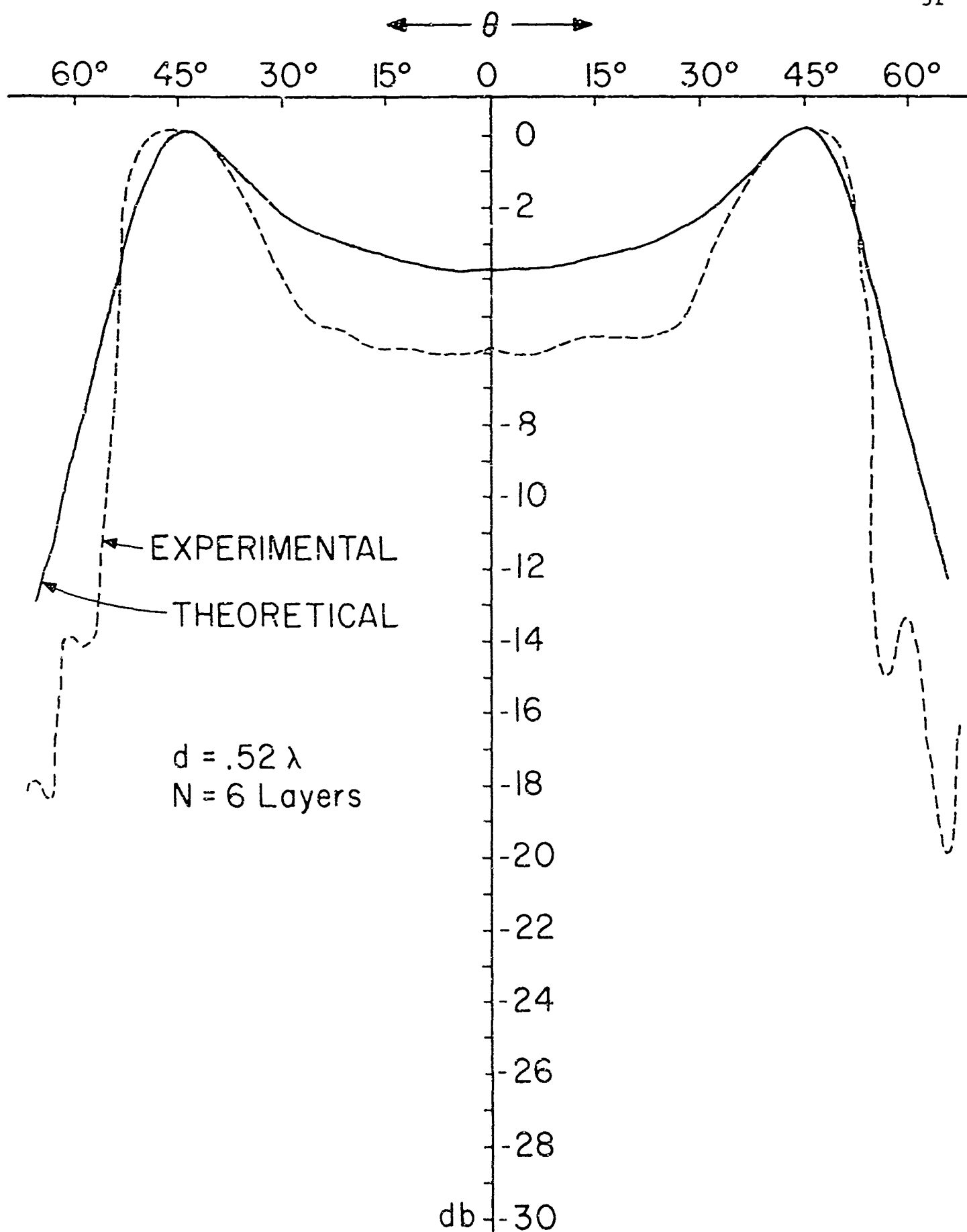


Fig. 8b Experimental and Theoretical Radiation Patterns for Infinite Inhomogeneous Plasma Sheath (6 Layers)

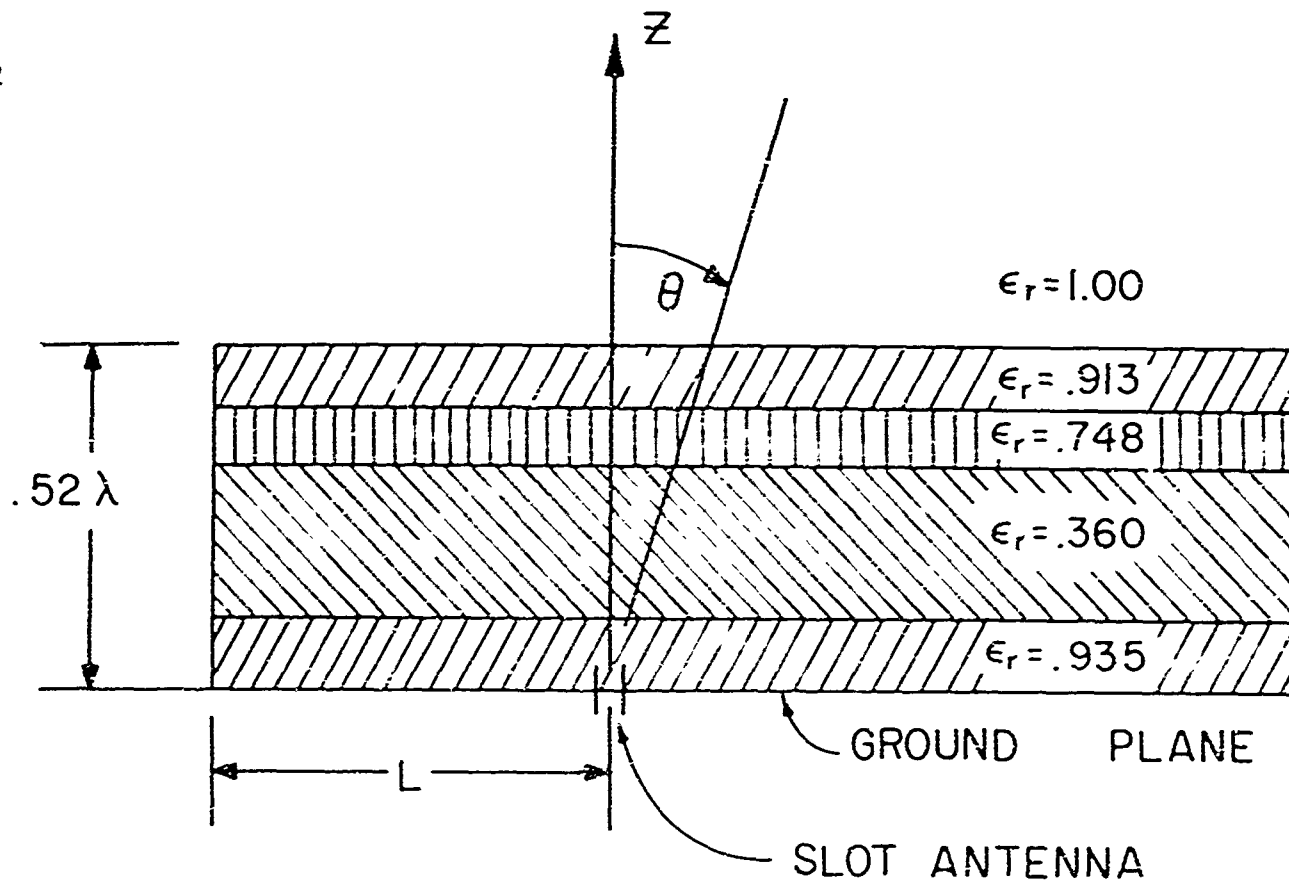


Fig. 9a Semi-Infinite Inhomogeneous Plasma Sheath Geometries

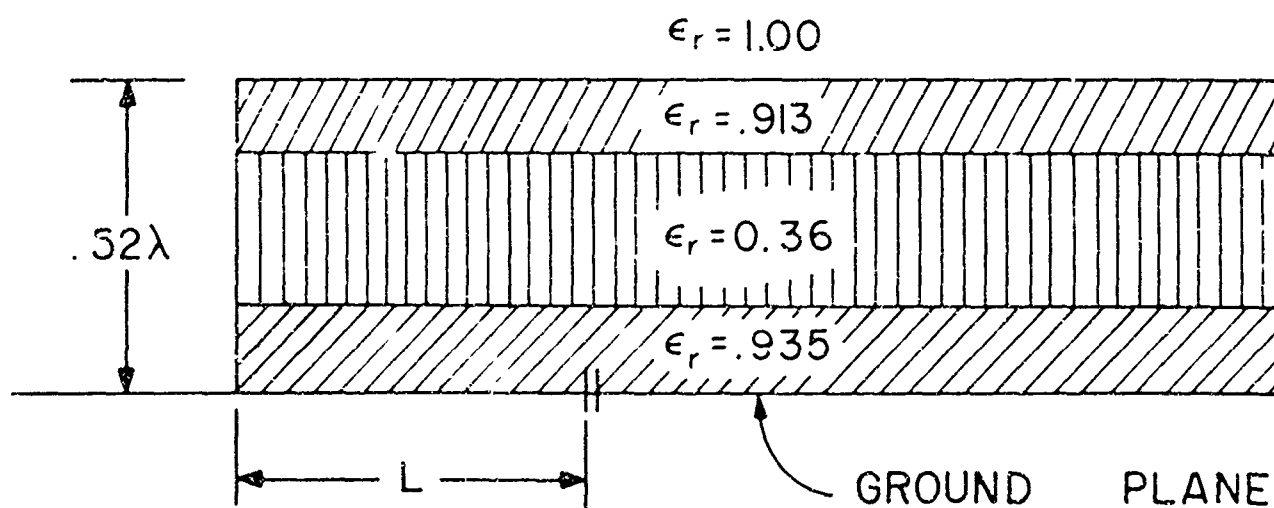


Fig. 9b Semi-Infinite Inhomogeneous Plasma Sheath Geometries

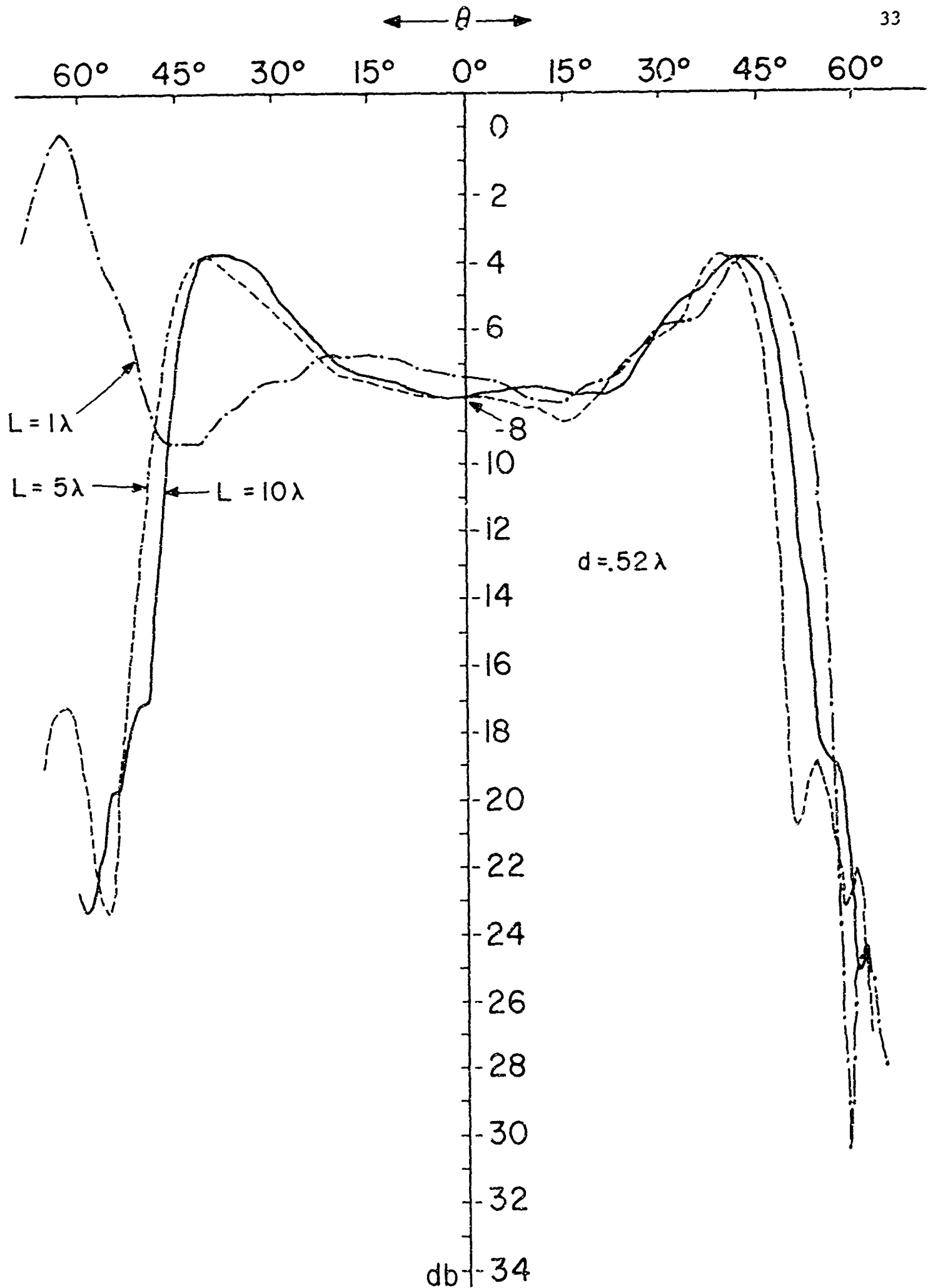
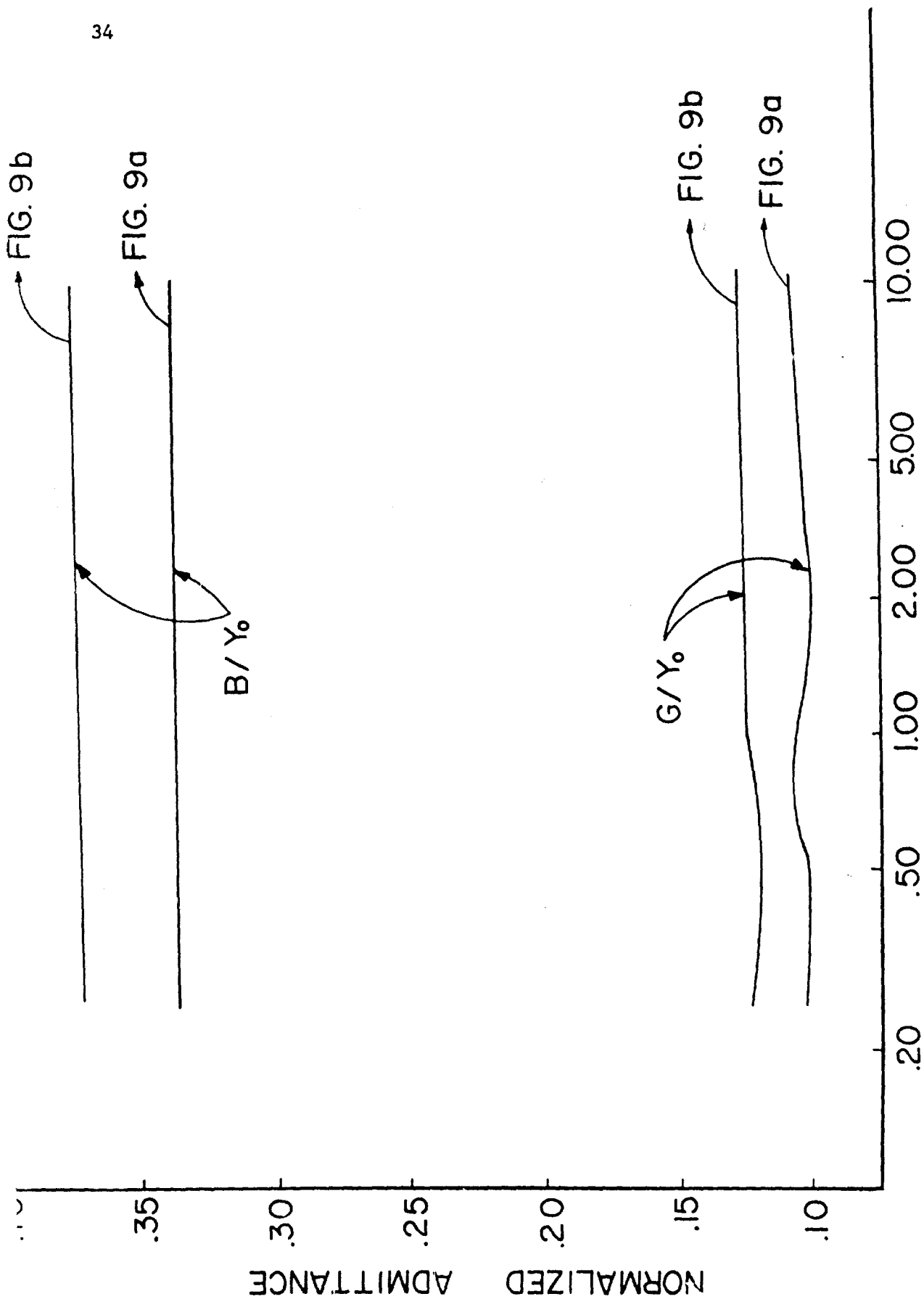


Fig. 10 Experimental Radiation Patterns for Semi-Infinite Inhomogeneous Plasma Sheath



DISCONTINUITY SEPARATION, L - (WAVELENGTHS)

Fig. 11 Admittance Characteristic for Semi-Infinite Inhomogeneous Plasma Sheath

5. References

- Rusch, W. V. T. (January, 1964), Radiation from an axially slotted cylinder with a radially inhomogeneous plasma coating, Canadian Journal of Physics, Vol. 42, 26-42.
- Tamir, T., and A. A. Oliner (January, 1962), The influence of complex waves on the radiation field of a slot-excited plasma layer, IRE Trans. on Antennas and Propagation, Vol. AP-10, No. 1, 55-65.
- Tamir, T., and A. A. Oliner, (1964), Radiation from semi-infinite slot-excited plasma sheath configurations, Electromagnetic Aspects of Hypersonic Flight (Second Symposium on the Plasma Sheath), Spartan Books, Incorporated, Baltimore, Maryland; 32-48.
- Tyras, G., P. C. Bargeliotis, J. M. Hamm, and R. R. Schell (June, 1965a), An experimental study of plasma sheath effects on antennas, Radio Sci. J. Res. NBS/USNC-URSI, Vol. 69D, No. 6, 839-850.
- Tyras, G. (1965b), On the excitation of electromagnetic waves in inhomogeneous media, Paper to be presented at the Symposium on Electromagnetic Wave Theory-Delft, September, 1965.

Unclassified

Security Classification

DOCUMENT CONTROL DATA - R&D		
<i>(Security classification of title, body of abstract and indexing annotation must be entered when the overall report is classified)</i>		
1. ORIGINATING ACTIVITY <i>(Corporate author)</i> Engineering Experiment Station The University of Arizona Tucson, Arizona		2a. REPORT SECURITY CLASSIFICATION Unclassified
		2b. GROUP
3. REPORT TITLE FURTHER EXPERIMENTAL STUDY OF PLASMA SHEATH EFFECTS ON ANTENNAS		
4. DESCRIPTIVE NOTES <i>(Type of report and inclusive dates)</i> Scientific Report (Interim) Jan. 1965 - July, 1965		
5. AUTHOR(S) <i>(Last name, first name, initial)</i> Tyras, G., and Hamm, John M.		
6. REPORT DATE July, 1965	7a. TOTAL NO. OF PAGES 40	7b. NO. OF REFS 5
8a. CONTRACT OR GRANT NO. AF19(628)-3834	9a. ORIGINATOR'S REPORT NUMBER(S) #2	
b. PROJECT and Task 464202		
c. DOD Element No. 62405304	9b. OTHER REPORT NO(S) <i>(Any other numbers that may be assigned this report)</i> AFCRL-65-608	
d. DOD Subelement No. 674642		
10. AVAILABILITY/LIMITATION NOTICES Qualified requestors may obtain copies of this report from DDC. Other persons or organizations should apply to the Clearinghouse for Federal Scientific and Technical Information (CFSTI), Sills Building, 5285 Port Royal Road, Springfield, Virginia 22151.		
11. SUPPLEMENTARY NOTES Simulation of Plasma Sheath	12. SPONSORING MILITARY ACTIVITY Hq. AFCRL, OAR (CRD) United States Air Force L.G. Hanscom Field, Bedford, Mass.	
13. ABSTRACT The plasma sheath simulation technique developed earlier has been used to investigate the effects of various types of sheath discontinuities and inhomogeneities on a slot antenna radiation pattern and input impedance. (U) In the case of semi-infinite and finite-extent homogeneous plasma sheaths, the radiation pattern and the impedance characteristic are investigated with regard to the geometry of the discontinuity and its proximity to the slot antenna. It is found that the radiation pattern is unaffected by the discontinuity as long as its distance from the slot is greater than 10 wavelengths. When the sheath is made finite in extent, with a discontinuity on each side of the slot, the resulting pattern is seen to be a superposition of the effects of each discontinuity acting separately. Investigation of the input impedance of the slot shows essentially no variation with discontinuity separation for separations larger than one wavelength. For smaller separations, the impedance exhibits significant variations, strongly dependent on the geometry of the discontinuity. The effects produced by inhomogeneities are found to be similar to those of a homogeneous sheath with a certain equivalent dielectric constant. For both the homogeneous and inhomogeneous sheaths, favorable comparison with the available theory is obtained. (U)		

DD FORM 1473
1 JAN 64

Unclassified

Security Classification

14. KEY WORDS	LINK A		LINK B		LINK C	
	ROLE	WT	ROLE	WT	ROLE	WT
Plasma simulation technique	8	3				
Discontinuities and inhomogeneities	6	2				
Radiation pattern and impedance	7	2				
Finite and semi-infinite sheath			8	3		
Discontinuity geometry			6	2		
Discontinuity separation			6	2		
Major lobe broadening			7	2		
Superposition of effects			7	2		
Sheath inhomogeneities			8,6	2		
Similar effects			7	2		
Favorable comparison					8,2	3

INSTRUCTIONS

1. ORIGINATING ACTIVITY. Enter the name and address of the contractor, subcontractor, grantee, Department of Defense activity or other organization (*corporate author*) issuing the report.

2a. REPORT SECURITY CLASSIFICATION. Enter the overall security classification of the report. Indicate whether "Restricted Data" is included. Marking is to be in accordance with appropriate security regulations.

2b. GROUP. Automatic downgrading is specified in DoD Directive 5200.10 and Armed Forces Industrial Manual. Enter the group number. Also, when applicable, show that optional markings have been used for Group 3 and Group 4 as authorized.

3. REPORT TITLE. Enter the complete report title in all capital letters. Titles in all cases should be unclassified. If a meaningful title cannot be selected without classification, show title classification in all capitals in parenthesis immediately following the title.

4. DESCRIPTIVE NOTES. If appropriate, enter the type of report, e.g., interim, progress, summary, annual, or final. Give the inclusive dates when a specific reporting period is covered.

5. AUTHOR(S). Enter the name(s) of author(s) as shown on or in the report. Enter last name, first name, middle initial. If military, show rank and branch of service. The name of the principal author is an absolute minimum requirement.

6. REPORT DATE. Enter the date of the report as day, month, year, or month, year. If more than one date appears on the report, use date of publication.

7a. TOTAL NUMBER OF PAGES. The total page count should follow normal pagination procedures, i.e., enter the number of pages containing information.

7b. NUMBER OF REFERENCES. Enter the total number of references cited in the report.

8a. CONTRACT OR GRANT NUMBER. If appropriate, enter the applicable number of the contract or grant under which the report was written.

8b, 8c, & 8d. PROJECT NUMBER. Enter the appropriate military department identification, such as project number, subproject number, system numbers, task number, etc.

9a. ORIGINATOR'S REPORT NUMBER(S). Enter the official report number by which the document will be identified and controlled by the originating activity. This number must be unique to this report.

9b. OTHER REPORT NUMBER(S). If the report has been assigned any other report numbers (*either by the originator or by the sponsor*), also enter this number(s).

10. AVAILABILITY LIMITATION NOTICES. Enter any limitations on further dissemination of the report, other than those imposed by security classification, using standard statements such as:

- (1) "Qualified requesters may obtain copies of this report from DDC."
- (2) "Foreign announcement and dissemination of this report by DDC is not authorized."
- (3) "U. S. Government agencies may obtain copies of this report directly from DDC. Other qualified DDC users shall request through _____."

- (4) "U. S. military agencies may obtain copies of this report directly from DDC. Other qualified users shall request through _____."

- (5) "All distribution of this report is controlled. Qualified DDC users shall request through _____."

If the report has been furnished to the Office of Technical Services, Department of Commerce, for sale to the public, indicate this fact and enter the price, if known.

11. SUPPLEMENTARY NOTES. Use for additional explanatory notes.

12. SPONSORING MILITARY ACTIVITY. Enter the name of the departmental project office or laboratory sponsoring (*paying for*) the research and development. Include address.

13. ABSTRACT. Enter an abstract giving a brief and factual summary of the document indicative of the report, even though it may also appear elsewhere in the body of the technical report. If additional space is required, a continuation sheet shall be attached.

It is highly desirable that the abstract of classified reports be unclassified. Each paragraph of the abstract shall end with an indication of the military security classification of the information in the paragraph, represented as (TS), (S), (C), or (U).

There is no limitation on the length of the abstract. However, the suggested length is from 150 to 225 words.

14. KEY WORDS. Key words are technically meaningful terms or short phrases that characterize a report and may be used as index entries for cataloging the report. Key words must be selected so that no security classification is required. Identifiers, such as equipment model designation, trade name, military project code name, geographic location, may be used as key words but will be followed by an indication of technical context. The assignment of links, rules, and weights is optional.